

ABSTRACT

CARUSO, BRUNO JUDE. The Temperature Effect on the Irradiation Induced Phase Change in Gallium Oxide. (Under the direction of Dr. Djamel Kaoumi).

Gallium oxide is rising as a material of interest in the semiconductor industry today for the use in high power electronic devices. Its ultra-wide bandgap, high breakdown field and irradiation hardness give it a competitive edge over the current semiconductors used in high power electronic devices. One application, in particular, is the use of Ga_2O_3 as a detection medium in high power UV detectors. The use of these detectors in high temperature/high dose environments requires an assessment and understanding of the irradiation behavior of the detection medium. Current literature observes a phase change in Ga_2O_3 under relatively low doses of ion irradiation at room temperature. However, the identification of the resulting phase has varied across these studies. The goal of this study is to identify the transformed phase at room temperature through electron microscopy, and to observe the effect of higher temperatures on the phase change. Through in situ Kr^{++} ion irradiation of Transmission Electron Microscopy (TEM) samples it is determined that a dose of less than 1 dpa at room temperature and 150°C induces a phase change from β - Ga_2O_3 to a mixture of κ - and γ - Ga_2O_3 which proves to be stable with time. The β -phase remains stable during irradiation experiments done at 300°C up to a dose of 6.74dpa.

© Copyright 2023 by Bruno Jude Caruso

All Rights Reserved

The Temperature Effect on the Irradiation Induced Phase Change in Gallium Oxide

by
Bruno Jude Caruso

A thesis submitted to the Graduate Faculty of
North Carolina State University
in partial fulfillment of the
requirements for the degree of

Master of Science

in

Nuclear Engineering

Raleigh, North Carolina
2023

APPROVED BY:

Djamel Kaoumi

Elizabeth Kautz

Rajeev Gupta

BIOGRAPHY

Bruno Jude Caruso was born in 2000 in the southwest suburbs of Chicago to parents Mary and Frank Caruso. He grew up in a small suburb right outside Chicago called Lemont which is the site of the country's first national laboratory, Argonne. This was always fascinating to Bruno, and from a young age he took a strong liking to math and science as a way to better understand and explain the world around him.

After high school, Bruno attended the University of Illinois in Champaign-Urbana where he received his Bachelor of Science in Nuclear Engineering. Upon graduation, he continued his education at North Carolina State University in pursuit of his Master's of Science in Nuclear Engineering. His experience as a researcher and experimenter grew rapidly with newfound skills operating electron microscopes and conducting in-situ material testing.

It is Bruno's goal to continue doing research that furthers the understanding of nuclear materials and educates the public on the beneficial uses of nuclear technology.

ACKNOWLEDGMENTS

I would like to first acknowledge my advisor Dr. Djamel Kaoumi who gave me the opportunity to be a part of his research group and pursue my Master's degree. I am thankful for his support and encouragement in learning TEM sample preparation and characterization techniques as well as in-situ experimentation. I want to extend my gratitude to Dr. Angelica Lopez Morales and my colleagues Matt DeJong and Dmitry Kretov who greatly contributed to the sample preparation and data collection presented in this thesis.

I want to express my gratitude as well to the IVEM staff including Pete Baldo and especially Wei-Ying Chen for their assistance during in-situ ion irradiation experiments performed at Argonne National Laboratory.

I would also like to acknowledge the Analytical Instrumentation Facility (AIF) staff at NC State. A special thank you to Christopher Winkler, TEM Lab Manager of the AIF, for his hard work and attentiveness which made it possible to acquire high-quality TEM and EELS data. Thanks also to Roberto Garcia, FIB Lab Manager, for training and assisting during TEM sample preparation.

I want to thank Dr. Farida Selim and her group at Bowling Green State University as well as Dr. Ben Derby and Kevin Baldwin for supplying me with high quality samples to conduct my research with.

I would like to thank my committee members Dr. Elizabeth Kautz and Dr. Rajeev Gupta for their time, suggestions, and support and to all the professors who have served in my classes. Special thanks are extended to the entire team within the nuclear engineering department whose collective efforts contribute to elevating this program into a source of pride for its students.

I also want to acknowledge my colleagues and friends Fu-Yun Tsai, Ertugrul Demir, Fedi Fehri, Philip Alarcón-Furman, and Saikumaran Ayyappan. It has been my pleasure to work with a group of such intelligent people and I am thankful for all of the help and insight you all provide on a daily basis.

My gratitude is as well for the Nuclear Science and Security Consortium for funding my degree and this study under award number DE-NA0003996. I would like to also thank DOE NSUF for providing us access to the IVEM facility

A very special thank you to my family, friends, and my girlfriend Claudia for their unconditional support and confidence in me throughout my move to North Carolina and pursuit of my Master's degree. I wouldn't have been able to do it without you.

TABLE OF CONTENTS

LIST OF TABLES	v
LIST OF FIGURES	vi
Chapter 1: Introduction	1
Chapter 2: Literature Review	3
2.1 Material Phases and Properties.....	3
2.2 Applications.....	5
2.3 Methods of Synthesizing Gallium Oxide	7
2.4 Radiation Effects	11
2.4.1 Neutron Irradiation.....	11
2.4.2 Swift Heavy Ion Irradiation	13
2.4.3 Proton Irradiation	14
2.5 Monoclinic to Orthorhombic Phase Change Under Irradiation	17
Chapter 3: Experimental Methods	24
Chapter 4: Results	28
4.1 Room Temperature Results	28
4.2 High Temperature Results.....	33
4.2.1 CZ Undoped Ga ₂ O ₃ Irradiated at 300°C	33
4.2.2 CZ Fe-Doped Ga ₂ O ₃ Irradiated at 150°C	33
4.2.3 EFG H-Doped Ga ₂ O ₃ Irradiated at 100°C and 300°C	34
Chapter 5: Discussion	36
5.1 Verification of Phase Change.....	36
5.2 Effect of Temperature	45
5.3 Effect of Dopant	47
5.4 Effect of Thickness.....	48
5.5 Mechanism of Phase Change	48
Chapter 6: Conclusion	53

LIST OF TABLES

Table 2.1	The investigated samples with thickness of component layers	19
Table 3.1	Experimental conditions for the different samples tested in this study.....	27
Table 5.1	Crystallographic information for Ga ₂ O ₃ polymorph phases of interest.....	44
Table 5.2	Error calculation for the specific volumes of undamaged Ga ₂ O ₃ polymorphs found in figures 5.6 and 5.8 relative to experimental data in PDFs	45

LIST OF FIGURES

Figure 2.1	Schematic diagram for the unit cell of β -Ga ₂ O ₃ along the c-(I), a-(II), and b-axis(III)	4
Figure 2.2	Empirical relationship between mean displacement energy E_d , and inverse lattice parameter for various semiconductors	4
Figure 2.3	The application fields of gallium oxide	6
Figure 2.4	Schematic of Verneuil growth equipment	7
Figure 2.5	Schematic of Czochralski growth equipment	8
Figure 2.6	Schematic of edge-defined film growth equipment. (a) The melt wets the die and is drawn up the capillary; (b) the seed is contacted to the melt and pulled up and cooling starts to increase the crystal size; (c) the crystal reaches the size of the die	9
Figure 2.7	Schematic of physical vapor deposition (PVD) chamber with radiofrequency (RF) power supply	10
Figure 2.8	Temperature dependence of the electrical conductivity before (°) and after irradiation (•) at various temperatures	12
Figure 2.9	Temperature dependence of the Seebeck coefficient of β -Ga ₂ O ₃ before (°) and after irradiation (•).....	12
Figure 2.10	Time dependence of the electrical conductivity of irradiated Ga ₂ O ₃ at various temperatures.....	13
Figure 2.11	PV-TEM images of β -Ga ₂ O ₃ lamella samples after SHI irradiation.....	14
Figure 2.12	Normalized latent track diameter distribution for β -Ga ₂ O ₃ lamella samples under different S_e values	14
Figure 2.13	Schematics of the Si implanted β -Ga ₂ O ₃ photodiode under a UV lamp.....	15
Figure 2.14	SRIM simulation for proton irradiation into β -Ga ₂ O ₃ photodiode (top left), zoomed in simulation of shallow region (top right), and average vacancies of gallium and oxygen within the Si implanted β -Ga ₂ O ₃ region as a function of different proton irradiation doses (bottom)	16
Figure 2.15	Real-time current of the Si implanted β -Ga ₂ O ₃ photodiode biased at 5V and illuminated with 254 nm ultraviolet light with intensity of 760 μ W/cm ² before and after (a) 1×10^{13} cm ⁻² and (b) 1×10^{15} cm ⁻² proton irradiation, respectively	16

Figure 2.16	Ion-beam-induced β - κ phase transformation in Ga ₂ O ₃ . (a) XRD 2theta scans of the sample implanted with 400keV ⁵⁸ Ni ⁺ ions as a function of ion dose. (b)The corresponding RBS/C spectra with the random and virgin spectra shown for comparison. (c) ABF-STEM image of β -Ga ₂ O ₃ sample irradiated with 1x10 ¹⁶ Ni/cm ² . Panels (d) and (e) illustrate SAED patterns from the unimplanted and implanted regions respectively. (f)-(h) FFTs from high-resolution images taken from different regions of the sample as indicated in the panel	18
Figure 2.17	Cross-sectional images of the annealed samples S1-550, S2-550, S3-600 and S4 600 showing the different thicknesses of the top and intermediate layers	20
Figure 2.18	Detailed HRTEM image of the interface between the top and intermediate layers in the S1-550 sample (a) and a sketch (b) of the lattice crystal growth continuity from the monoclinic phase to the orthorhombic phase.....	20
Figure 2.19	(a) HRTEM image of the bottom layer in the S4-600 sample, showing a coherent lattice of the HfO ₂ structure which gradually changes from the monoclinic to orthorhombic structure. (b) A similar image obtained in plan view specimen from the same sample	21
Figure 2.20	GIXRD of as-deposited and annealed HfO ₂ films.....	23
Figure 3.1	TANDEM-IVEM Facility at Argonne National Lab showing path of ion beam from the source to the TEM room (top left to bottom). Schematic of the setup geometry inside of the microscope (top right)	24
Figure 3.2	Depth profile (left) and damage profile (right) of Ga ₂ O ₃ under 1MeV Kr ⁺ irradiation output from SRIM simulation.....	25
Figure 3.3	Brightfield TEM images of the four samples at room temperature before irradiation	26
Figure 4.1	Sequence of electron diffraction patterns and bright field image acquired for (a) CZ β -Ga ₂ O ₃ Fe-doped, (b) EFG β -Ga ₂ O ₃ H-doped, and (c) CZ β -Ga ₂ O ₃	28
Figure 4.2	Selected area electron diffraction patterns from post irradiation examination of (a) CZ Fe-Doped Ga ₂ O ₃ , (b) EFG H-Doped Ga ₂ O ₃ , and (c) a simulation overlaying the [001] κ -Ga ₂ O ₃ (orange) and [111] γ -Ga ₂ O ₃ (red).....	29
Figure 4.3	Full indexation of the κ -phase (a) and γ -phase (b) for the EFG H-doped sample irradiated to 3.5dpa at room temperature.....	30

Figure 4.4	(a) Full indexation of the κ -phase (orange) and γ -phase (red) for the CZ undoped sample irradiated to 3.5dpa at room temperature and (b) simulation of [001] γ -phase and [794] κ -phase patterns overlaid on one another	31
Figure 4.5	EELS spectra of the oxygen K edge, acquired from (a) unirradiated β -Ga ₂ O ₃ H-doped and corresponding irradiated sample (b) unirradiated β -Ga ₂ O ₃ undoped and corresponding irradiated sample.	32
Figure 4.6	SAED acquired for the gallium oxide samples irradiated with 1 MeV Kr ions at RT (a) SAED corresponding to the initially β -Ga ₂ O ₃ CZ-Ga ₂ O ₃ sample (b) SAED corresponding to the initially β -Ga ₂ O ₃ Fe-doped and (c) SAED corresponding to the initially β -Ga ₂ O ₃ H-doped acquired one year after the experiment was performed. ...	32
Figure 4.7	Diffraction patterns for CZ grown undoped Ga ₂ O ₃ along with Single Crystal β -Ga ₂ O ₃ pattern with zone axis [101].....	33
Figure 4.8	TEM image with indicated selected area (left), electron diffraction patterns (middle), and Single Crystal© patterns of corresponding β -Ga ₂ O ₃ and κ -Ga ₂ O ₃ (right) for CZ Fe-Doped sample	34
Figure 4.9	TEM image with indicated selected area (left), electron diffraction patterns (middle), and Single Crystal© pattern of β -Ga ₂ O ₃ at zone axis [15 $\bar{8}$] (right) for EFG H-Doped sample.....	35
Figure 4.10	TEM image with indicated selected area (left), electron diffraction patterns (middle), and Single Crystal© patterns of corresponding β -Ga ₂ O ₃ and κ -Ga ₂ O ₃ (right) for EFG H-Doped sample	35
Figure 5.1	Experimental patterns on different zone axes from the CZ Fe-doped sample irradiated to 4.03dpa at 150°C along with simulated patterns of mixed κ -Ga ₂ O ₃ (orange) and γ -Ga ₂ O ₃ (red)	38
Figure 5.2	Full indexation of different zone axis pattern for CZ Fe-doped sample irradiated to 4.03dpa at 150°C.....	39
Figure 5.3	Lattice total energy vs volume per formula unit for six different Ga ₂ O ₃ polymorphs obtained with DFT calculations	40
Figure 5.4	Theoretical scenario of two unit cells being irradiated with 1MeV Kr ions. The two unit cells are shown in pristine condition at the start of irradiation (left) and in the damaged state after irradiation (right).....	41
Figure 5.5	Comparison of the DFT, soapGAP and tabGAP energies for the five experimentally identified $\beta/\kappa/\alpha/\delta/\gamma$ polymorphs. In the overall plot (a), the gray shadow region	

	corresponds to the energy-crossing region magnified and compared closely in (b, c, d).	43
Figure 5.6	Comparison of diffraction patterns for EFG grown H-doped samples irradiated at 300°C, 100°C and room temperature along with simulated electron diffraction patterns for the indexed phases	46
Figure 5.7	High magnification bright field TEM images of Ga ₂ O ₃ film on NaCl at room temperature (a) and at 600°C (b) along with corresponding electron diffraction patterns	49
Figure 5.8	Low magnification bright field TEM images of Ga ₂ O ₃ film at room temperature (a) and at 800°C (b) along with corresponding electron diffraction patterns	51

CHAPTER 1: Introduction

Gallium oxide is currently on the forefront of research in the semiconductor industry. Gallium oxide fills a gap in the semiconductor applications due to the specific properties of the different phases/structures that it is present in. Ga_2O_3 is a great candidate for the ultra-high power market due to its ultra-wide band gap. This market has different applications, but due to the material properties of Ga_2O_3 , the focus is on high-power solar blind UV detectors. As a result, the Ga_2O_3 will be exposed to high levels of radiation as well as high temperature which can affect its material properties and behavior as a semiconductor. It is also envisioned as a detection material in nuclear applications. For this reason, it is important to analyze the behavior of gallium oxide under these extreme conditions.

In this study, three bulk gallium oxide samples were grown using two different methods: edge-defined film-fed growth (EFG) and Czochralski growth (CZ). The EFG grown sample was doped with hydrogen while one of the CZ grown samples was iron doped and the other CZ grown sample was undoped. Lamellar TEM samples were processed with a gallium Focused Ion Beam (FIB) for all three samples. The lift outs were characterized on TEM and irradiated in-situ at Argonne on the Intermediated Voltage Electron Microscope (IVEM). Irradiation was first carried out at room temperature and subsequently done at higher temperatures (100 – 300°C) in order to substantiate the temperature effect. Room temperature irradiation reveals the initiation of a phase change from $\beta\text{-Ga}_2\text{O}_3$ to $\kappa\text{-Ga}_2\text{O}_3$ in all samples, while the completion of the phase only occurred in the EFG grown H-doped sample. Analysis of the room temperature data led to the hypothesis that the phase change is controlled by defect accumulation that raises the free energy of the damaged $\beta\text{-Ga}_2\text{O}_3$ to a higher value than the free energy of the $\kappa\text{-Ga}_2\text{O}_3$. Irradiation done at 300°C showed no sign of a phase change occurring which supports the idea that the phase change is controlled by the

accumulation of defects. To further investigate the hypothesis, more Ga_2O_3 samples were produced, however this time they were grown as thin films through physical vapor deposition (PVD).

CHAPTER 2: Literature Review

2.1 Material Phases and Properties

Before diving into semiconductor applications and radiation induced microstructural changes, it is first important to understand the properties and phases of gallium oxide. Gallium oxide is present in six different phases: $\alpha, \beta, \gamma, \delta, \varepsilon$ and κ [1]. The crystalline structure for the phases are rhombohedral, monoclinic, cubic, body-centered cubic, orthorhombic, and orthorhombic respectively. κ -Ga₂O₃ presents an orthorhombic structure (Pna21 space group symmetry 33) whereas γ -Ga₂O₃ presents a cubic structure (Fd-3m space group symmetry 221). The κ -phase has been recognized to be a subgroup of ε -Ga₂O₃ which pertains to the hexagonal P63mc space group [2]. According to density functional theory (DFT) calculation of the total lattice energies of the Ga₂O₃ polymorphs [3] and calculation of the Helmholtz free energies [4] the stability of the gallium oxides polymorphs increases in the following order $\delta < \varepsilon < \gamma < \alpha < \kappa < \beta$. Of these six phases, the most thermodynamically stable phase is the monoclinic β -Ga₂O₃ as shown in figure 2.1. The other phases are metastable, and should transform into the more stable form, β -Ga₂O₃, at temperatures above 750-900°C [5]. To determine the thermodynamic stability, the inverse of the lattice parameter is related to the displacement energy of the structure. For β -Ga₂O₃ the lattice constants are as follows: $a = 12.2\text{\AA}$, $b = 3.0\text{\AA}$, and $c = 5.8\text{\AA}$. As a very rough estimate, the average of lattice constants b and c is taken to be 4.4\AA whose inverse is 0.227 [6]. This inverse lattice constant is then related to the displacement energy E_d through the plot shown in figure 2.2. Based on the relation shown on the plot, β -Ga₂O₃ has a displacement energy, or radiation hardness,

similar to that of GaN. What separates β -Ga₂O₃ from materials of similar displacement energies is its thermal conductivity. β -Ga₂O₃ has a thermal conductivity that is about half that of sapphire and an order of magnitude lower than GaN [5]. Due to its monoclinic nature, the β -Ga₂O₃ also exhibits anisotropy in its thermal conductivity [7].

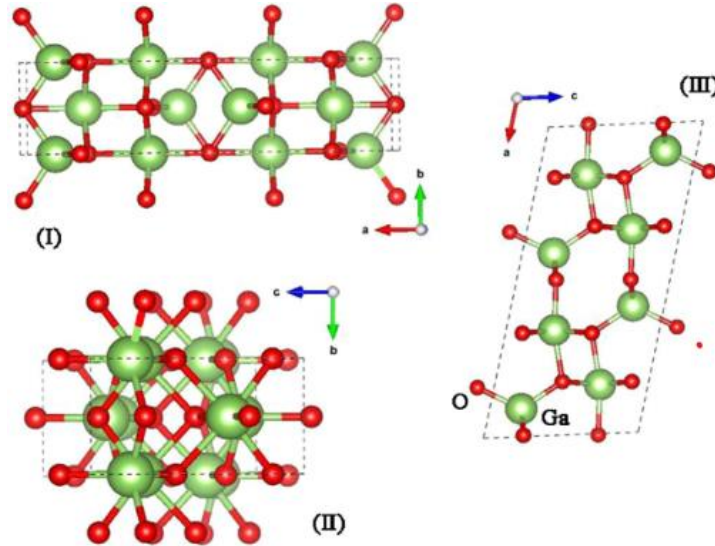


Figure 2.1 Schematic diagram for the unit cell of β -Ga₂O₃ along the c-(I), a-(II), and b-axis(III) [7]

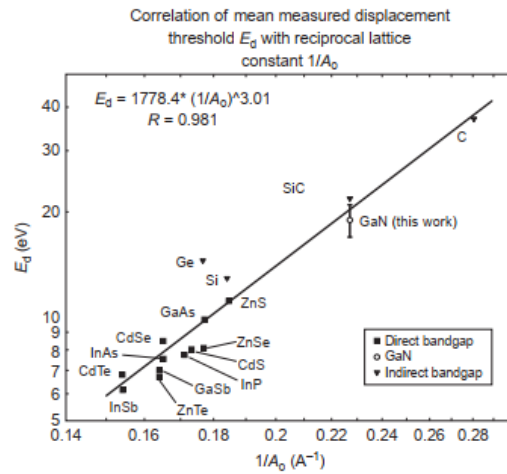


Figure 2.2 Empirical relationship between mean displacement energy E_d , and inverse lattice parameter for various semiconductors [6]

As previously mentioned, β -Ga₂O₃ is also desirable for its ultra-wide bandgap of around 4.8-4.9eV [8]. This means that the Ga₂O₃ has a relatively large energy difference between electrons in its valence band and its conduction band. This inherently makes Ga₂O₃ an insulator. However, β -

Ga₂O₃ has a fundamental absorption edge of 250nm, meaning that the concentration of electrons in the conduction band is increased through the absorption of deep UV rays. This allows the Ga₂O₃ to meet the “conductivity requirement” and act as a conductor [7]. This can also be achieved by doping or production under reducing conditions which can allow for the increase of free electrons and thus an increase in conductivity [5]. In addition to its ultra wide bandgap, Ga₂O₃ also has a high breakdown field of around 8MV/cm [8]. This is the voltage of an electric field needed to strip the material of its electrons and cause it to begin to ionize. The Ga₂O₃ breakdown field is higher in comparison to similar wide bandgap materials like silicon carbide (SiC) and gallium nitride (GaN), which makes it favorable for high power, high frequency devices [8].

2.2 Applications

Gallium oxide has a vast range of applications from its use as a detection medium in the semiconductor industry to its implementation as a drug carrier in the biomedical industry. The application space as presented by Shi and Qiao [7] is shown in figure 2.3. For the scope of this report the focus is on the application of gallium oxide as a photodiode in solar-blind UV detectors. Solar blind UV detectors, as the name implies, are “blind” to photons with a wavelength longer than 280nm. This is useful in allowing the detection of deep UV rays without the interference of infrared or visible light, usually from the sun or room lighting. UV detectors, just like gallium oxide, have their own wide range of applications including but not limited to astronomical studies, fire alarms, missile-warning systems, inter-satellite communications and emitter calibration. In the past, UV detectors relied on photomultiplier tubes which are very delicate and require the use of high voltage sources making them large, heavy and expensive. These detectors have since been improved with solid-state alternatives like ultraviolet-enhanced, Si-based photodetectors. However, Si-based photodetectors also come with drawbacks as they need expensive optical filters

to compensate for their narrow bandgap. In turn they cannot operate in the high-temperature, radioactive environments that they are needed in. For these harsh environment applications, Ga_2O_3 prevails with the help of a wider bandgap and lower absorption edge [9].

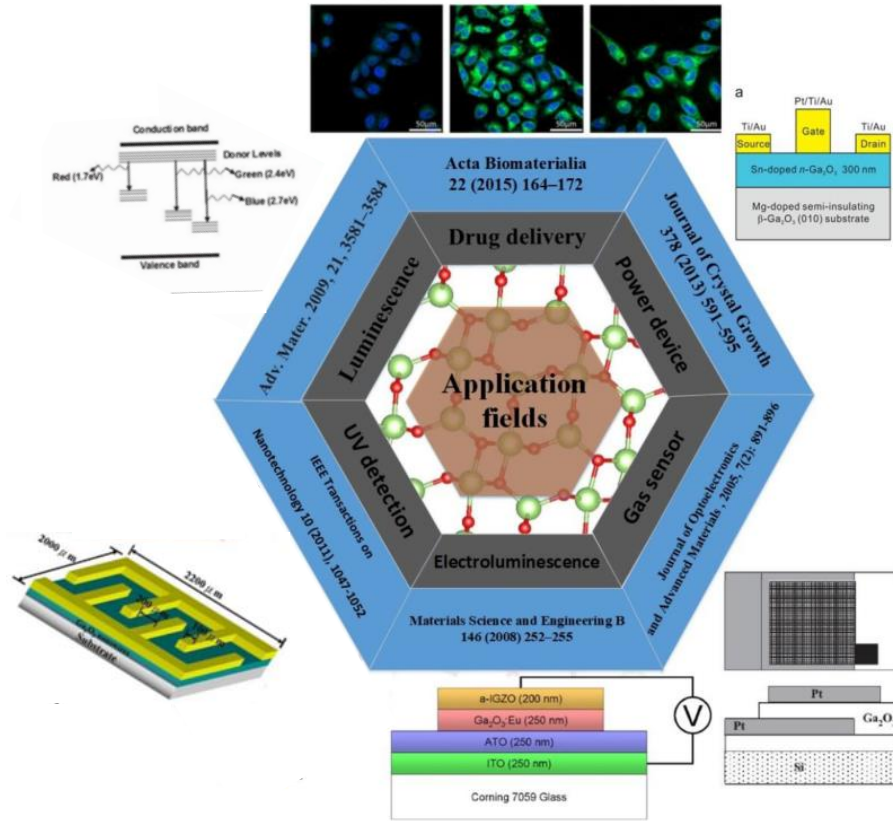


Figure 2.3 The application fields of gallium oxide [7]

In these UV detectors, Ga_2O_3 works as a semiconductor. However, as discussed earlier, the properties of Ga_2O_3 classify it as an insulator. In a perfect crystal this would hold true, but in reality single crystal gallium oxide wafers contain unintentional silicon impurities from the powder source that make it n-type [10]. In order to control its conductive properties, the material must be processed or prepared in a certain way. Conductive properties of gallium oxide can be controlled through n- or p-type doping, and through synthesis under reducing conditions [11]. Doping is the implantation of ions in order to induce a donor or acceptor into the lattice. Donors offer a free electron whereas acceptors offer a hole. In gallium oxide, gallium is a 3^+ ion and the oxygen is a

2-. In order to create an n-type semiconductor the sample must be doped with an ion that has a positive charge lower than 3^+ , for instance H^+ and He^+ can be used to replace a gallium ion in the lattice and “create” a free electron. On the other hand, p-type doping is very difficult in gallium oxide because oxides tend to form donor type oxygen vacancies causing n-type conduction. This technique, however, can be very beneficial to create a homogeneous gallium oxide p-n junction. Another way to increase conductivity in gallium oxide is through synthesis in reducing conditions [11]. In other words, if gallium oxide is grown in an environment with limited oxygen, the lattice will naturally form with oxygen vacancies that cause n-type conduction.

2.3 Methods of Synthesizing Gallium Oxide

Gallium oxide can be synthesized in many ways to produce either high quality bulk material or gallium oxide thin films. For the purpose of its application as a semiconductor, gallium oxide needs to be single crystal, pure in phase, and absent of defects, so the means of production is very important. A few of the most common bulk synthesis methods are Verneuil, Czochralski (CZ), and edge-defined film fed growth (EFG) [12]. Verneuil growth is shown in figure 2.4.

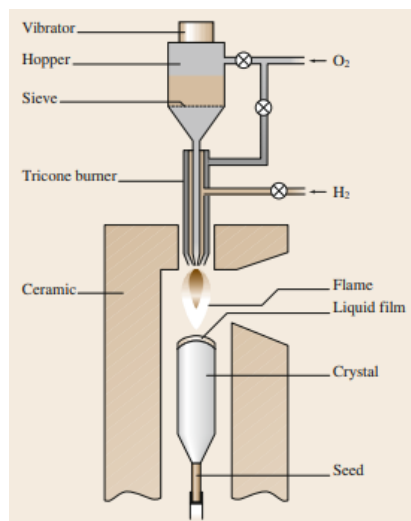


Figure 2.4 Schematic of Verneuil growth equipment [13]

Verneuil is the fastest growth method and the first one that can control nucleation. For this reason, Verneuil growth can produce large crystals for high melting point materials. To begin, a heat source, most commonly an oxy-hydrogen flame, heats a seed crystal on a ceramic pedestal. Powder is shaken through the flame by a hopper and forms a melt surface on the seed crystal. The melt surface gradually solidifies on the seed crystal causing the material to take on the crystal structure of the seed. The lowering of the seed crystal determines the linear growth rate, and the powder feed rate determines the volumetric growth rate. This process is convenient, but can lead to high dislocation densities and concentration variations [13].

Czochralski is also a fast growth method that normally produces almost perfect and homogenous crystals. However, this process only applies to materials that melt congruently, in other words the solid and melt compositions are the same at equilibrium. A schematic of the Czochralski setup is shown in figure 2.5. To start the process, a solid form of the desired crystal is placed in a crucible, and it is heated to several degrees above the melting temperature.

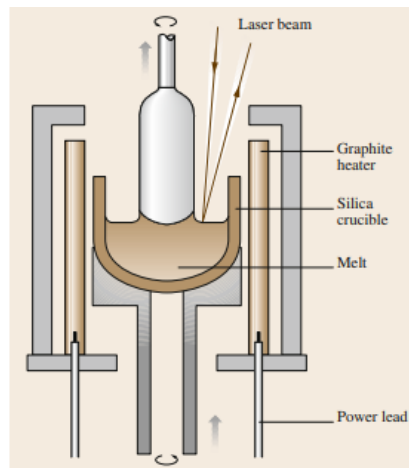


Figure 2.5 Schematic of Czochralski growth equipment [13]

A rotating seed crystal is lowered to come into contact with the melt surface. The seed crystal begins to melt and after a few minutes, pulling is started. Initially the temperature is held constant and as the seed crystal is removed a long neck region is grown to reduce dislocation density. The

melt temperature is then reduced to increase the diameter of the crystal. Once the desired diameter and length are reached, the growth can be stopped by swiftly increasing the pull rate or increasing the melt temperature to reduce the diameter to zero [13].

Another growth process that is commonly used is “edge-defined film-fed” growth. In the same way a material is melted to create a melt pool. A die with a central capillary is put in contact with the melt surface. Surface tension forces the melt surface to wet the die and get drawn up the capillary as shown in figure 2.6. At this point a seed crystal is lowered to touch the melted material in the capillary and the pulled upward. The temperature is lowered to increase the crystal diameter until it reaches the die diameter. The die allows for the production of various shapes of crystals, for example, tubes, sheets, etc.[13]

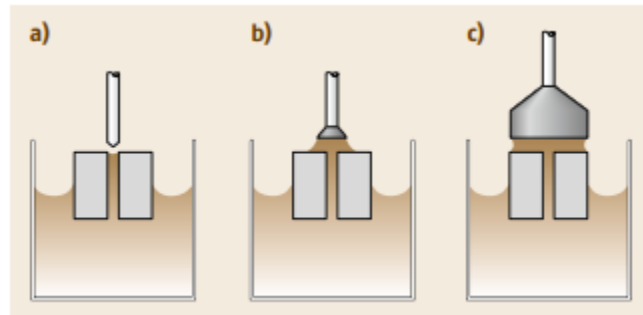


Figure 2.6 Schematic of edge-defined film growth equipment. (a) The melt wets the die and is drawn up the capillary; (b) the seed is contacted to the melt and pulled up and cooling starts to increase the crystal size; (c) the crystal reaches the size of the die [13]

Gallium oxide can also be fabricated in the form of thin films. One of the most common way to make these thin films is through physical vapor deposition (PVD). Figure 2.7 shows a schematic of a PVD chamber using a radio frequency (RF) power supply. PVD chambers can operate using DC or RF power supplies. DC power supplies apply a direct current to the system to create a voltage bias between the chamber walls and the target. For targets that are not conductive, however, a DC power supply cannot be used. For these purposes an RF power supply is needed.

RF power supplies alternate the voltage between being positive and negative in the form of a sine wave. The high voltage excites the neutral Argon atoms into an Argon plasma composed of free electrons and positively charged Argon ions [14]. Since the Ar^+ ions are positively charged they are accelerated at the target when the voltage being output by the RF power supply is negative. The accelerated Ar^+ ions hit the target and transfer their kinetic energy to the target atoms. Sputtering in the target occurs when the target atoms received enough energy to break their bonds and get ejected from the target material. These atoms are sputtered in every direction meaning that some of them are ejected in the direction of the substrate. To ensure that the deposition is uniform the substrate is rotated during sputtering to counteract the random nature of the sputtering.

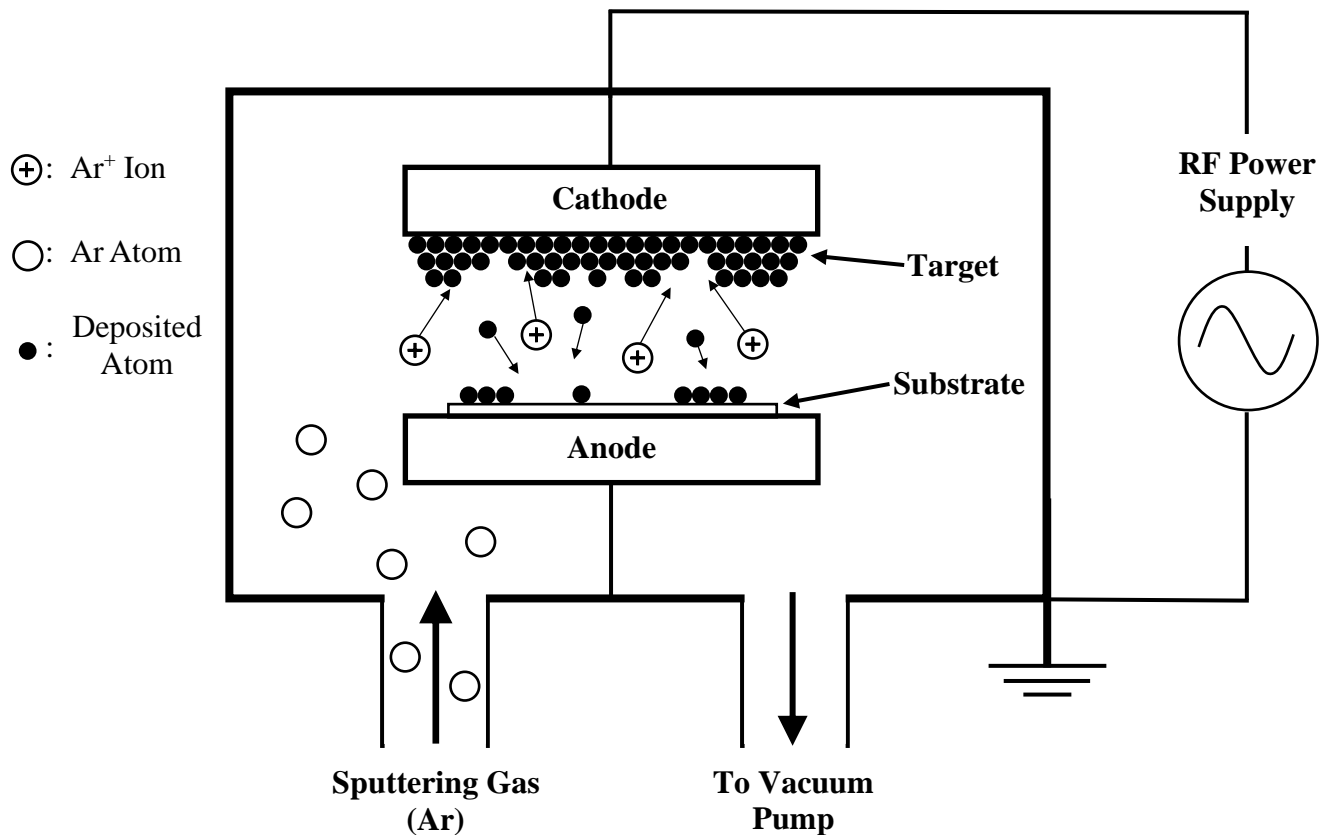


Figure 2.7 Schematic of physical vapor deposition (PVD) chamber with radiofrequency (RF) power supply (adapted from [14])

2.4 Radiation Effects

In order to consider the use of gallium oxide for detection in nuclear environments, it is useful to understand the effect that irradiation has on the structure and properties of gallium oxide. This will provide insight as to how its behavior as a semiconductor will change. Ga_2O_3 is expected to be inherently resilient to radiation because oxides typically have stronger interatomic bonding. This can help to limit damage, but eventually all materials are affected by irradiation. Since, UV detectors can be anywhere from in your school fire alarm to inside orbital satellites it is important to consider all types of radiation and their effects on gallium oxide.

2.4.1 Neutron Irradiation

A study was performed by Cojocaru to determine the effect of fast neutrons on the conductivity and thermoelectric power of $\beta\text{-Ga}_2\text{O}_3$ [15]. The samples were prepared by pressing powder into cylindrical pellets. The pellets were then sintered for 10 hours at 1300K to form pure $\beta\text{-Ga}_2\text{O}_3$. The samples were irradiated inside of a 2MW reactor at a neutron flux of $6 \times 10^{12} \text{ n.cm}^{-2}\text{s}^{-1}$ and at temperatures of 373K, 523K, and 673K. One way that the defect production and migration is studied in the material is through measuring the conductivity at varying temperatures. The temperature range for the conductivity measurements in this experiment was 600K to 1000K. The rate of increase was constant and equal to 0.62K/s. The neutron flux was integrated over time to yield a particle fluence of $4 \times 10^{17} \text{ n.cm}^{-2}$. Figure 2.8 shows the temperature dependence of the conductivity for the three irradiated samples and one unirradiated sample as $\log(\sigma)$ vs reciprocal temperature. It can be shown in the plot that the conductivity decreases by over an order of magnitude from irradiation and as the plot approaches higher temperatures the decrease begins to disappear. At around 950K the difference in conductivity between the irradiated and unirradiated samples completely disappears. Figure 2.9 shows the time dependence of electrical conductivity.

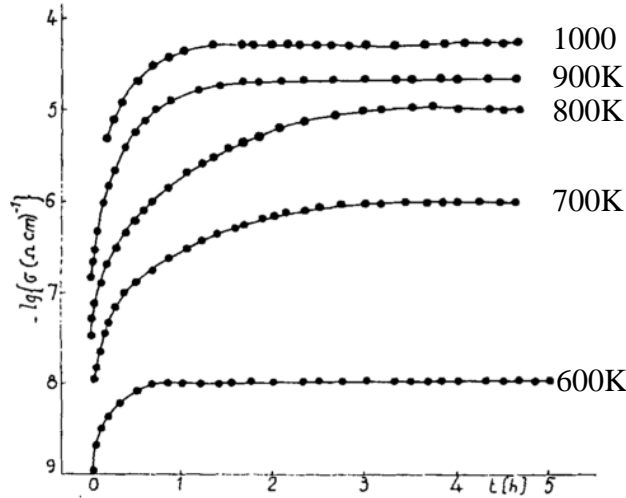


Figure 2.8 Temperature dependence of the electrical conductivity before (°) and after irradiation (•) at various temperatures [15]

At 600K there is no significant change in conductivity. However, at 700K there is a slight increase in conductivity over time and at 800K and above there is a significant increase in conductivity.

The final measurement was performed on the thermoelectric power of the samples before and after irradiation. As shown in figure 2.8, the thermoelectric power increases by a factor of two due to neutron irradiation. The change in conductivity that is seen after irradiation can be explained by

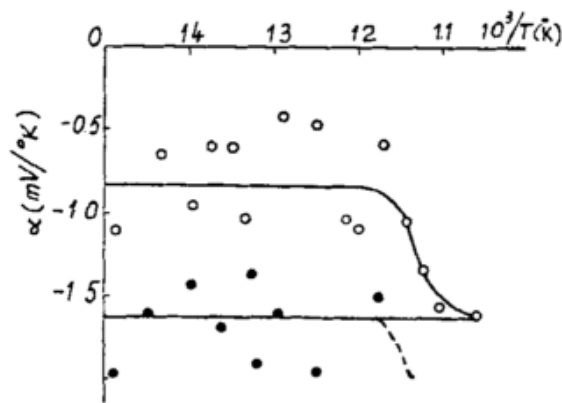


Figure 2.9 Temperature dependence of the Seebeck coefficient of β -Ga₂O₃ before (°) and after irradiation (•) [15]

the presence of Frenkel defects in the lattice that act as trapping sites for electrons. This decreases the number of electrons present in the conduction band and therefore decreases the conductivity.

It is determined from figure 2.10 that the mobility of defects increases strongly for annealing above

800°C for the first three hours. Below this temperature the annealing process is slow and insignificant [15].

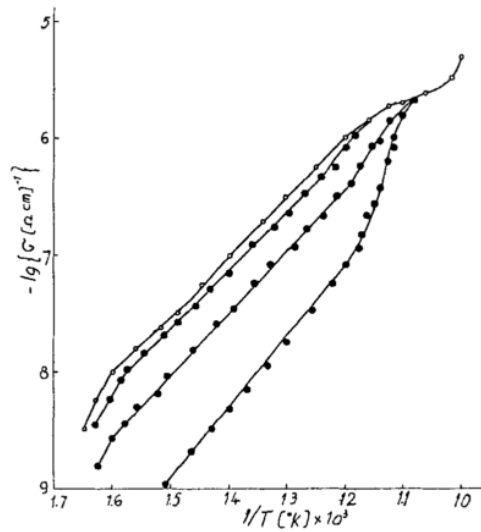


Figure 2.10 Time dependence of the electrical conductivity of irradiated Ga₂O₃ at various temperatures [15]

2.4.2 Heavy Ion Irradiation

Materials respond much differently to swift heavy ions (SHI) as opposed to neutrons, electrons or gammas. SHI irradiation results in widespread ionization and electron excitation in materials, which causes a region of the sample, several nanometers in diameter, to be structurally modified. This is called a latent track or ion track [8]. For these experiments, β -Ga₂O₃ samples were irradiated in-situ on a TEM with 5-10 MeV.u⁻¹ ¹⁸¹Ta and ⁸⁶Kr ions. Figure 2.11 shows images of the lamellar samples after ion irradiation where S_e is the electronic energy loss. The dark circles that can be seen on the surface of the samples show the formation of a latent track inside of the oxide (they appear elliptical in figure 2.11.i because sample is tilted 15° in respect to electron beam). After analysis it was concluded that the dark spots corresponded to the ion irradiation induced tracks. The electronic energy loss was related to the diameter of the latent track and plotted in figure 2.12. The cross section of the latent tracks increases linearly as a function of the electronic energy loss. Using this information, a threshold electron energy loss (S_e) can be calculated to

determine the minimum electronic loss necessary to create a latent track. By extrapolating the relationship between latent track diameter and S_e , the minimum electronic energy loss was determined to be around 16.3 keV nm^{-1} [8].

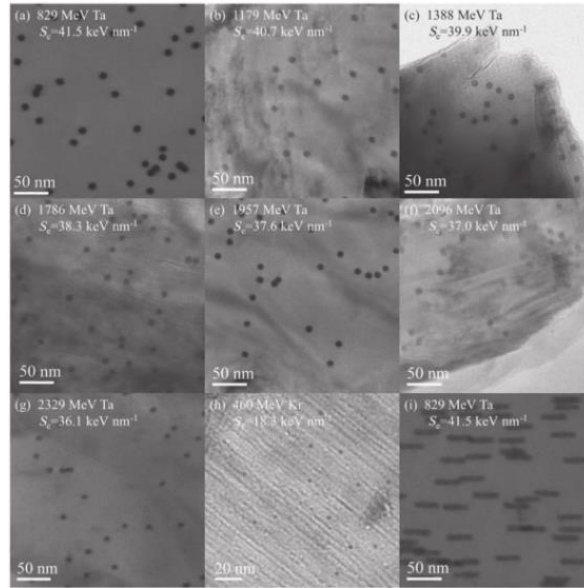


Figure 2.11 PV-TEM images of $\beta\text{-Ga}_2\text{O}_3$ lamella samples after SHI irradiation [8]

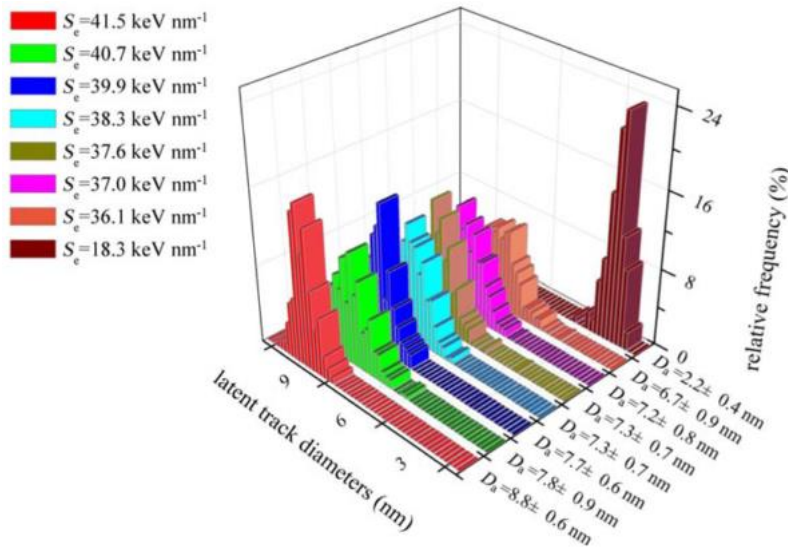


Figure 2.12 Normalized latent track diameter distribution for $\beta\text{-Ga}_2\text{O}_3$ lamella samples under different S_e values [8]

2.4.3 Proton Irradiation

Shihyun Ahn et. al performed an experiment to observe the effect of 5MeV proton irradiation on the performance of photodetectors [16]. The photodetectors were fabricated using the schematics

shown in figure 2.13. The irradiation was at a fluence of 10^{13} to 10^{15} cm^{-2} at 25°C . This is the equivalent of many decades of exposure in low earth orbit, so it gives a realistic comparison to the real-life application of an inter-satellite communication device. At this energy the protons transmit through the gallium oxide wafer and pass into the sapphire substrate. SRIM simulations were performed as a comparison to the experimental results. Figure 2.14 shows the vacancy concentration as a function of depth in the wafer as estimated by SRIM, along with the experimental results.

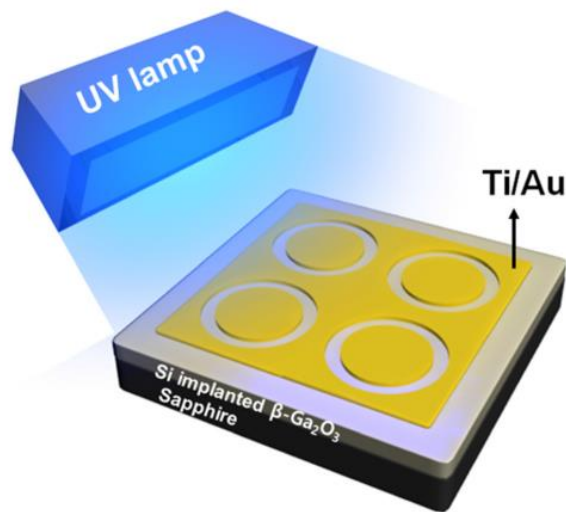


Figure 2.13 Schematics of the Si implanted $\beta\text{-Ga}_2\text{O}_3$ photodiode under a UV lamp [16]

It must be understood that the total vacancy estimations are an overestimate due to recombination. However, the estimations are useful to determine the amount of point defects that were initially created in the primary damage regime. After determining defect concentration, the effect of these defects was examined by plotting the photocurrent and dark current as a function of dose at room temperature and at 150°C for 254nm wavelength photons as shown in figure 2.15. The photocurrent and dark current are shown to increase after irradiation in all cases. This increase in photocurrent is more prevalent at the higher dose and can be explained by the presence of defect levels within the bandgap [16]. Although the photocurrent is increased after irradiation, the photo-

to-dark current ratio (PDCR) decreases. Even with this decrease in the PDCR, the detectors were still operational after the highest dose and show great potential for photodetection in harsh environments.

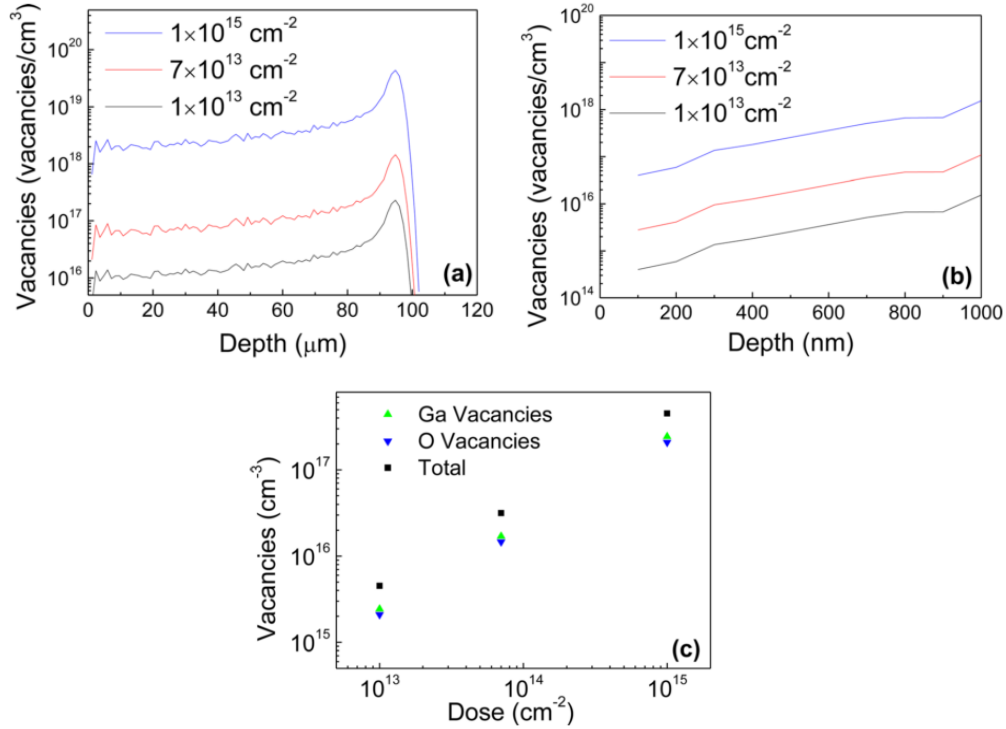


Figure 2.14 SRIM simulation for proton irradiation into $\beta\text{-Ga}_2\text{O}_3$ photodiode (top left), zoomed in simulation of shallow region (top right), and average vacancies of gallium and oxygen within the Si implanted $\beta\text{-Ga}_2\text{O}_3$ region as a function of different proton irradiation doses (bottom) [16]

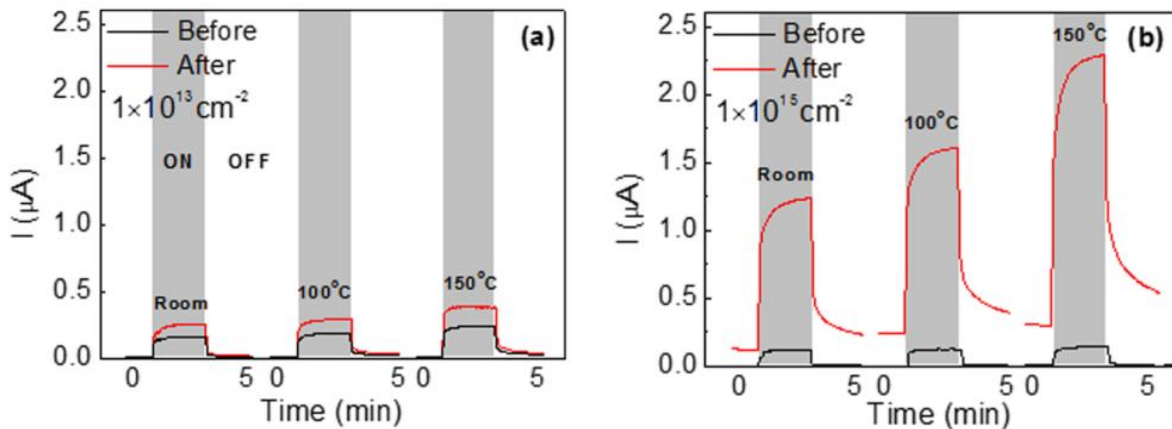


Figure 2.15 Real-time current of the Si implanted $\beta\text{-Ga}_2\text{O}_3$ photodiode biased at 5V and illuminated with 254 nm ultraviolet light with intensity of $760 \mu\text{W/cm}^2$ before and after (a) $1 \times 10^{13} \text{ cm}^{-2}$ and (b) $1 \times 10^{15} \text{ cm}^{-2}$ proton irradiation, respectively [16]

2.5 Monoclinic to Orthorhombic Phase Change Under Irradiation

β -Ga₂O₃ is monoclinic and under irradiation it has been reported first to transition to κ -Ga₂O₃ which is orthorhombic [3]. Multiple studies have shown this irradiation-induced change in phase to what is a metastable κ -Ga₂O₃ phase [6, 13, 15]. The mechanism behind the phase change is still unknown but there are several hypotheses on what the mechanism could be. Some studies propose that the implantation of ions is the mechanism behind the changing of phase [6]. Other studies propose that the strain induced by irradiation through implantation and the creation of defect structures are the cause of the phase change in gallium oxide.

A study by Azarov et. al. was aimed at uncovering this mechanism. In this study β -Ga₂O₃ wafers, obtained from Tamura Corporation, were irradiated to different fluences with three different incident ions [3]. Subsequently, a Focused Ion Beam was used to take samples from the wafers that capture the interface between the damaged region and the undamaged region. This depth was determined using SRIM to find the range of each ion in the gallium oxide. A combination of SAED, XRD, RBS and EELS showed that a phase change gradually occurred from 6×10^{13} to 1×10^{16} ions/cm² as shown in figure 2.16. The study concluded that the mechanism responsible for the phase change involved the lattice disorder-induced strain accumulation that provided the initial internal energy necessary to overcome a threshold. Above this threshold the material was able to relax to a lower, more stable energy state known as the κ -Ga₂O₃ [3].

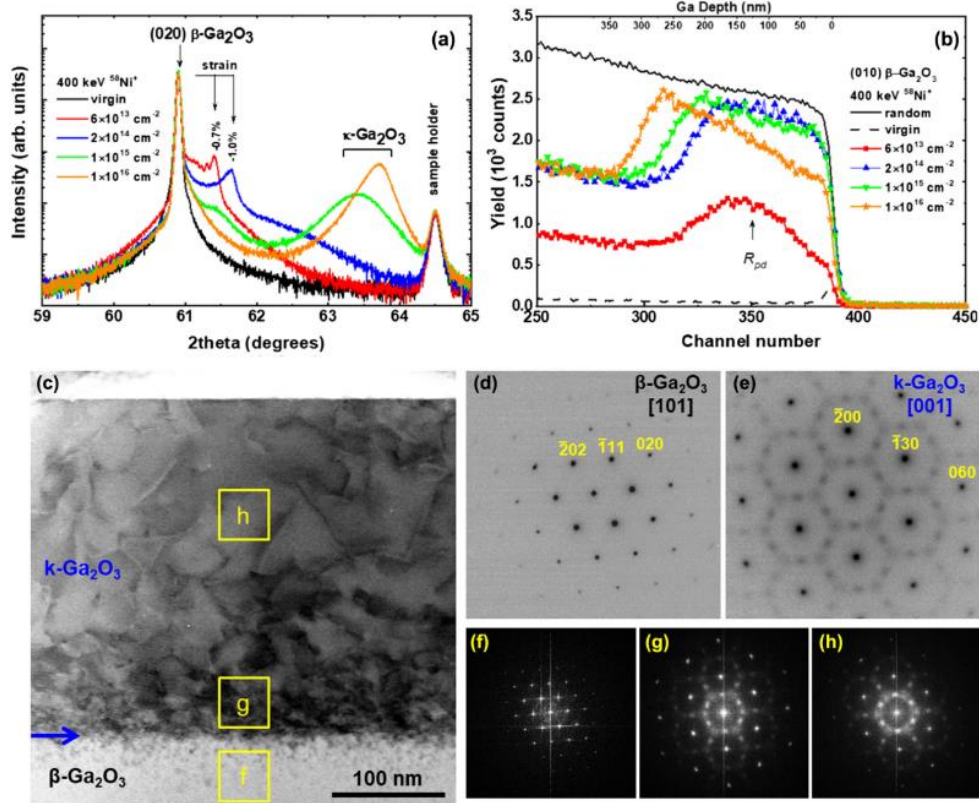


Figure 2.16 “Ion-beam-induced β - κ phase transformation in Ga_2O_3 . (a) XRD 2theta scans of the sample implanted with 400keV $^{58}\text{Ni}^+$ ions as a function of ion dose. (b)The corresponding RBS/C spectra with the random and virgin spectra shown for comparison. (c) ABF-STEM image of β - Ga_2O_3 sample irradiated with 1×10^{16} Ni/cm². Panels (d) and (e) illustrate SAED patterns from the unimplanted and implanted regions respectively. (f)-(h) FFTs from high-resolution images taken from different regions of the sample as indicated in the panel” [3].

Due to the limited amount of studies performed on irradiation induced phase change in Ga_2O_3 , the transition between monoclinic and orthorhombic structures in other materials can be studied to better understand the transition between β and κ in Ga_2O_3 . One example of this transition occurs in HfO_2 , a material that has potential for application as a ferroelectric memory device. A study done by Palade et. al. uncovers the mechanism behind the continuous transition between monoclinic and orthorhombic HfO_2 [17]. The ferroelectric properties of HfO_2 depend on many factors with one of them being crystalline structure. It has been found that the polar, orthorhombic non-centrosymmetric $Pca2_1$ phase is responsible for the ferroelectric properties found in HfO_2 . Similar to Ga_2O_3 , this orthorhombic phase is also metastable. Specific conditions of film thickness, grain size, surface and interface energy at grain boundaries, and dopant concentration allow for

the presence of the metastable phase. However, the most important condition for the stabilization of the orthorhombic phase seems to be the presence of vacancies. In terms of the stability of the ferroelectric phase after doping with Si and Ge, density functional theory simulations have shown that Si doping by itself is not enough to stabilize the orthorhombic phase. A specific spatial arrangement of dopant atoms in the microstructure of HfO₂ is required [17, 18].

In this study HfO₂ was fabricated in the form of a 3-layer memory structure composed of a Ge-rich Ge-HfO₂ thin film layer sandwiched between two thin films of pure HfO₂. The samples are listed in table 2.1 and were prepared by sputtering Ge and HfO₂ from different targets. The intermediate layer was held at a constant Ge content which was 70 vol%, or 79 at% Ge. Four different samples were created with varying thickness for the top and intermediate layers to optimize the monoclinic/orthorhombic ratio. Low magnification XTEM images show the thickness of each layer in each of the 4 samples in figure 2.17. In order to get a better understanding of the continuous spatial transition between the monoclinic and orthorhombic phases, high resolution TEM was performed on the interfaces of the three-layered system. It is shown in figure 2.18a that the top layer is in the monoclinic phase of HfO₂ oriented in the [110] zone axis.

Table 2.1 The investigated samples with thickness of component layers [17]

Sample	p-Si substrate resistivity [Ω cm]	Designed/ T_{RTA} [°C]	Label	d_{top} [nm]	d_{int} [nm]	d_{bot} [nm]	d_{int}/d_{top} [%]
S1	7-14	Designed	S1	60	10	10	16.7
		550	S1-550	57	10	11	17.5
		600	S1-600	57	8	11	14.0
S2	7-14	Designed	S2	60	20	10	33.3
		550	S2-550	57	22	13	38.6
		600	S2-600	65	19	13	29.2
S3	7-14	Designed	S3	24	7.5	10	31.3
		600	S3-600	25	6.5	9.5	26.0
S4	0.2-2.0	Designed	S4	30	15	10	50.0
		600	S4-600	23.5	15.5	12.5	66.0

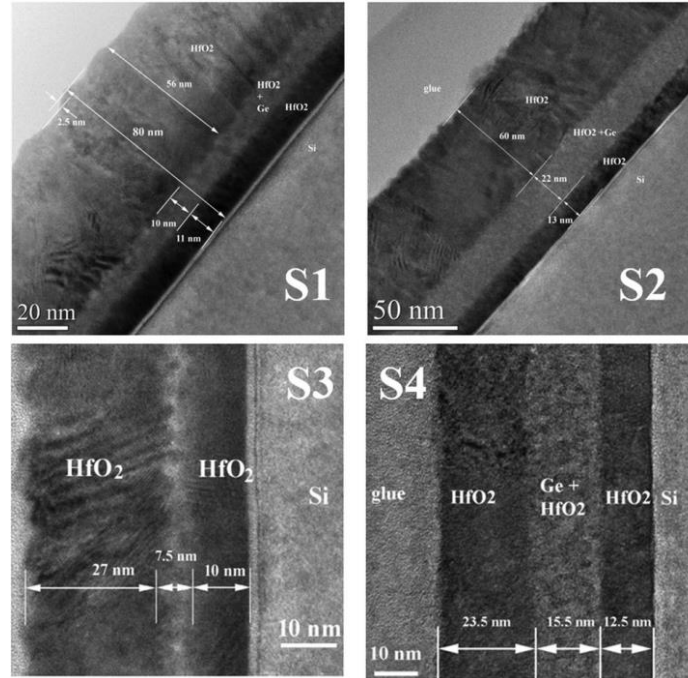


Figure 2.17 Cross-sectional images of the annealed samples S1-550, S2-550, S3-600 and S4-600 showing the different thicknesses of the top and intermediate layers [17]

The intermediate layer is identified as the orthorhombic phase of HfO_2 . The transition between phases keeps the (-111) lattice plane of the monoclinic lattice parallel to the (111) plane of the orthorhombic lattice [17]. For this case the deviation between the (111) plane of the monoclinic and the (111) plane of the orthorhombic is anywhere between 2.5° and 5° . This continuity in the (111) plane is why the phase transition is considered to be continuous between the layers.

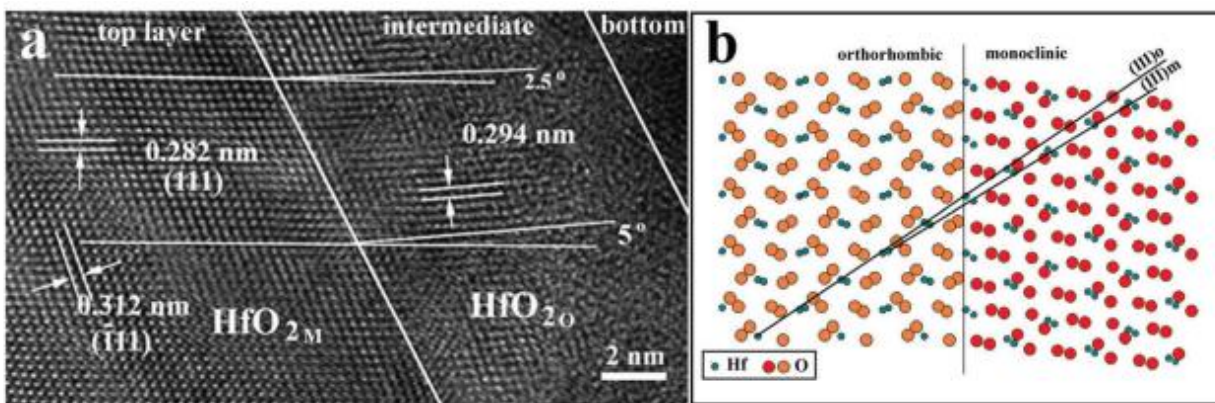


Figure 2.18 Detailed HRTEM image of the interface between the top and intermediate layers in the S1-550 sample (a) and a sketch (b) of the lattice crystal growth continuity from the monoclinic phase to the orthorhombic phase [17]

Another observation is that the orthorhombic phase only appears in the Ge-doped layer. This indicates that doping plays a major role in the transition and stabilization of phase from monoclinic to orthorhombic. The strain remaining after crystallization was also found to influence the crystalline state of the monoclinic and orthorhombic phases. This strain can be induced by dopant segregation and HfO_2 crystallization in the upper layers. Figure 2.19a shows the presence of strain in the bottom layer through alternating phase monoclinic-orthorhombic crystallites. The interplanar distances of these crystallites were measured and were shown to be different than the bulk interplanar distances. This gradual divergence from the bulk interplanar distance implies that the monoclinic and orthorhombic structures are under stress [17].

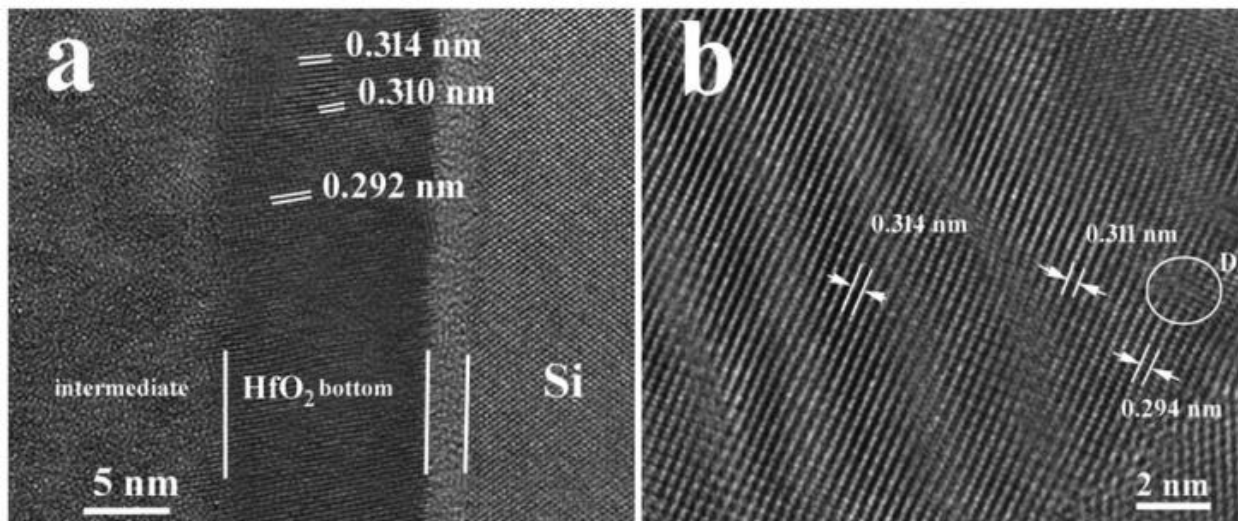


Figure 2.19 (a) HRTEM image of the bottom layer in the S4-600 sample, showing a coherent lattice of the HfO_2 structure which gradually changes from the monoclinic to orthorhombic structure. (b) A similar image obtained in plan view specimen from the same sample. [17]

Another study, done by Mittmann et al. on the monoclinic to orthorhombic phase change that occurs in HfO_2 , explores a phenomenon that shows promise as a candidate for the Ga_2O_3 phase change mechanism [18]. In this study, an HfO_2 target was sputtered by physical vapor deposition (PVD) to grow HfO_2 ferroelectric capacitors (FeCaps) under varying sputtering atmospheres, with oxygen flowrates ranging from 0 to 7.0 standard cubic centimeters per minute (sccm) and a constant argon flowrate of 20 sccm. The plasma power during sputtering was held constant at

200W. First it must be noted that, compared to atomic layer deposition (ALD), PVD has a higher chance to generate oxygen vacancies. Also, sputtering from a metal oxide target is expected to lead to the depletion of oxygen on the surface of the target and eventually a higher concentration of oxygen vacancies in the deposited film. This means that a film deposited with an oxygen flowrate of 0 sccm will naturally contain a high concentration of oxygen vacancies. By flowing oxygen in the chamber as the target is being sputtered, the concentration of oxygen in the PVD-deposited films increases which decreases the amount of oxygen vacancies. The as-deposited films have a mostly amorphous structure, so they were annealed at 800C for 20 seconds in order to give the lattice enough energy to crystallize. Figure 2.20 shows the GIXRD of the as-deposited and annealed films at the various oxygen flowrates. The first observation that can be made is that the as-deposited films are amorphous at low oxygen flowrate, but begin to show crystallinity at higher oxygen flowrates. This can be seen by a small wide peak, that is characteristic of an amorphous material,

transforming into a slightly more defined hump at around 28° that indicates the formation of small monoclinic crystallites. The higher oxygen flowrate decreases the deposition rate of the film which extends the film growth time allowing seed nucleation of the most stable HfO_2 phase, monoclinic [18]. After annealing, the actual structure of the films can be observed. The films that contain less oxygen align with the peaks given for orthorhombic and tetragonal phases of HfO_2 . Since it is difficult to distinguish between the peak angles of these two phases, the paper combines them and states it as the o + t phase. The films that contain more oxygen clearly align with the peaks for the monoclinic phase.

This change in phase with oxygen flowrate can be interpreted as a direct relationship between the concentration of oxygen vacancies and the material phase. Just like during the deposition of thin

films through PVD, oxygen vacancies are created during ion irradiation of Ga_2O_3 . Oxygen vacancies are preferentially created compared to gallium vacancies because the displacement energy of oxygen is lower than that of gallium. These oxygen atoms are kicked out of their lattice positions and migrate to interstitial positions in the monoclinic Ga_2O_3 structure. Once enough vacancies are accumulated it is more energetically favorable for the structure to transform into the orthorhombic $\kappa\text{-Ga}_2\text{O}_3$ phase just like the experiment on the HfO_2 . In order to test this hypothesis, the same experiment that was performed on the HfO_2 can be done on Ga_2O_3 to observe if the varying flowrate of oxygen yields this same phase change.

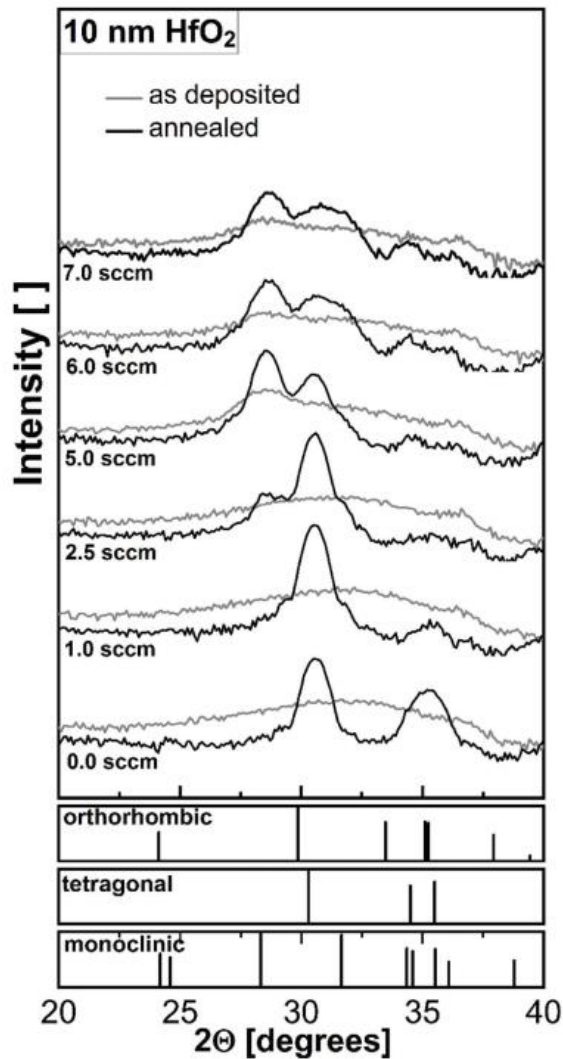


Figure 2.20 GIXRD of as-deposited and annealed HfO_2 films [18]

CHAPTER 3: Experimental Methods

To gain a better understanding of the mechanism behind the irradiation induced phase change in gallium oxide, our study was conducted using temperature as a varying parameter on the irradiation of lamellar TEM samples. Samples were irradiated at temperatures between 20 - 300°C using 1 MeV Kr^{++} ions at a rate of 150 cts/s. The energy of the Kr^{++} ions and the thickness of the Ga_2O_3 were such that ion implantation was negligible.

The irradiation was carried out at the TANDEM-IVEM facility at Argonne National Laboratory. The setup consists of a Krypton ion beam that is offset by 15° with an electron beam that is used for TEM imaging. The samples were tilted to an angle of 15° to ensure that the ion beam was incident with the Krypton beam. The source is located above the room with the microscope and an electrostatic deflector is used to divert the beam to the room below as shown in figure 3.1 [19]. A diagram also shown in figure 3.1 gives a schematic of the setup inside the microscope showing the offset of the Kr^+ beam from the electron beam.

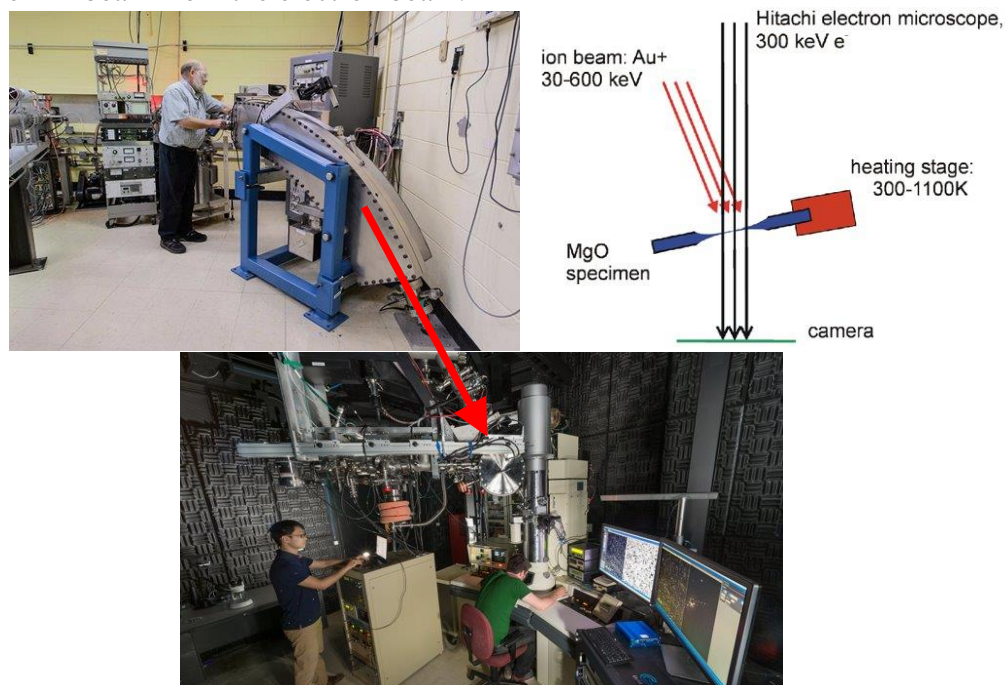


Figure 3.1 TANDEM-IVEM Facility at Argonne National Lab showing path of ion beam from the source to the TEM room (top left to bottom) [19]. Schematic of the setup geometry inside of the microscope (top right)

Using a program called The Stopping and Range of Ions in Matter (SRIM) the damage in a 100nm thick sample of Ga₂O₃ was simulated. SRIM uses a Monte Carlo simulation to model displacement cascades. Two different modes are available: “Full Cascade” and “Quick” mode [20]. The quick calculation mode was used. The program was run using a 1 μm thick sample of Ga₂O₃ and 1 MeV Kr⁺ ions. The displacement energy, E_d, for oxygen and gallium were 14eV and 28eV respectively [21]. The simulation was run for 100,000 ions at which point the damage profile and depth profile were obtained. The output is given in units of $\left[\frac{\text{displacements}}{\text{Angstrom}\cdot\text{ion}}\right]$ so it must be divided by the atomic number density to obtain the units of $\left[\frac{\text{displacements}\cdot\text{cm}^2}{\text{atom}\cdot\text{ion}}\right]$, or $\left[\frac{\text{dpa}}{\text{fluence}}\right]$. Now, for a specific desired dpa, the fluence necessary to reach it can be calculated. It was determined that the fluence necessary to reach 1dpa in a 100nm sample of Ga₂O₃ is around $4.64\text{E}+14 \left[\frac{\text{ions}}{\text{cm}^2}\right]$.

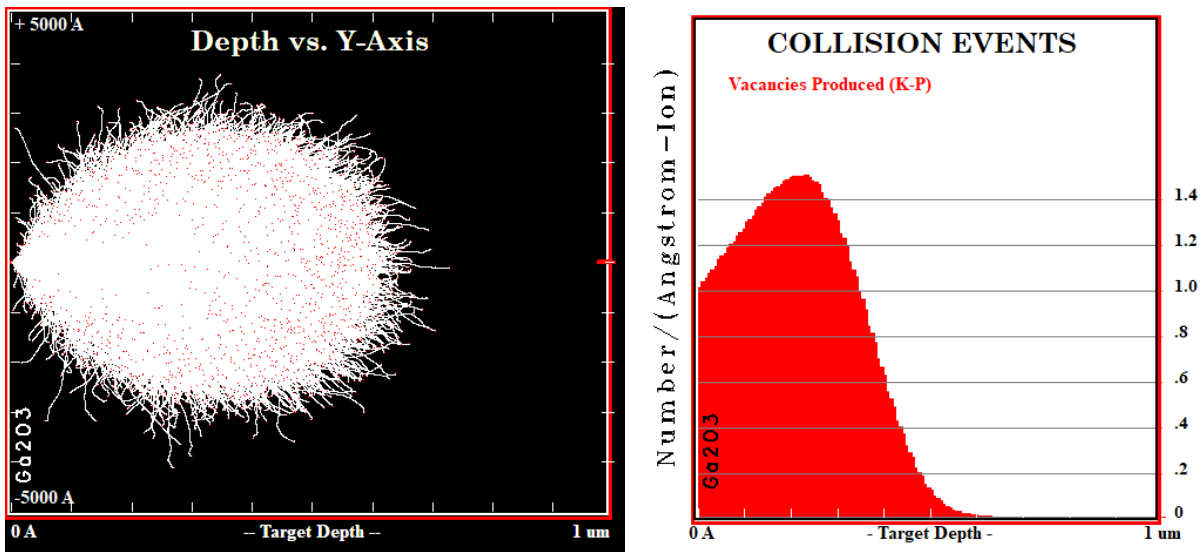


Figure 3.2 Depth profile (left) and damage profile (right) of Ga₂O₃ under 1MeV Kr⁺ irradiation output from SRIM simulation

Preliminary experiments at room temperature were performed by Dr. Lopez Morales on three different samples that were grown at Bowling Green State University using Czochralski (CZ) and Edge-defined Film-Fed Growth (EFG) techniques. Two of the three samples were grown using the CZ method. Of the two CZ samples, one was undoped and one was doped with Fe. The third

sample was grown using EFG and was doped with H. The flux was around 6.25×10^{11} ions/cm²s, all samples were irradiated to 3.5dpa, and all irradiation was done at room temperature to isolate the effect of implantation on phase change.

Using the FIB, four more TEM liftouts of the Ga₂O₃ bulk samples were taken to perform high temperature experiments that explore the effect of temperature on the phase change. The four samples are shown in figure 3.3 at room temperature, before irradiation. The images show that all four samples are single crystal and three of the samples have two windows of thickness. Selected area electron diffraction (SAED) patterns as well as TEM images were taken of all the samples before irradiation. The first sample to be irradiated was the CZ grown, undoped sample. The sample was heated to 300°C where images and SAED were taken to observe any changes due to heating. Once at temperature, the sample was irradiated to a dose of 4.03dpa. Diffraction patterns and images were taken along the way. The next sample to be irradiated was the CZ grown, Fe-doped sample. This sample was heated to 150°C where images and diffraction patterns were taken to observe any changes due to the heating. It was then irradiated to 4.03dpa at which point diffraction patterns and images were taken. The final two samples were both grown by EFG and doped with hydrogen. Table 3.1 shows the experimental conditions as well as the date of experimentation for all samples.

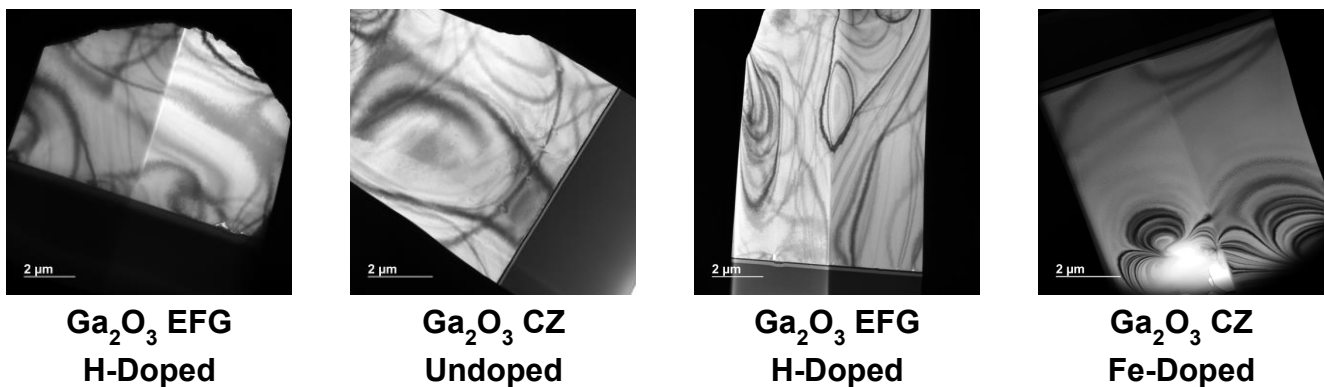


Figure 3.3 Brightfield TEM images of the four samples at room temperature before irradiation.

One of the EFG H-doped samples was heated to 300°C and irradiated to 6.75dpa. Diffraction patterns and images were taken after heating and at various doses along the way to the target dose. The other sample was going to be heated to 100°C to observe how the difference in temperature affects the stability of the β phase of Ga₂O₃. Due to FIB damage that was present, the sample was heated to 600°C to anneal any defects before cooling back down to 100°C and irradiating. Diffraction patterns were taken during heating. After cooling back down to 100°C the sample was irradiated to around 0.41dpa.

Table 3.1 Experimental conditions for the different samples tested in this study

Material	Growth Method	Dopant	Temperature of Irradiation [22]	Maximum Irradiation Dose [dpa]
β -Ga ₂ O ₃	CZ	Undoped	RT	3.5
β -Ga ₂ O ₃	CZ	Fe	RT	3.5
β -Ga ₂ O ₃	EFG	H	RT	3.5
β -Ga ₂ O ₃	CZ	Undoped	300	4.0
β -Ga ₂ O ₃	CZ	Fe	150	4.0
β -Ga ₂ O ₃	EFG	H	300	6.75
β -Ga ₂ O ₃	EFG	H	100	0.40

CHAPTER 4: Results

4.1 Room Temperature Results

Figure 4.1 illustrates brightfield images and diffraction patterns that were acquired for each of the room temperature samples at different doses [22]. Here the initial phase of the samples at 0 dpa was characterized as β -phase according to the selected area electron diffraction (SAED) analysis. The β -phase has a monoclinic structure with space group C2/m [15]. This phase is generally the most common one as it is the phase that presents the minimum energy of formation.

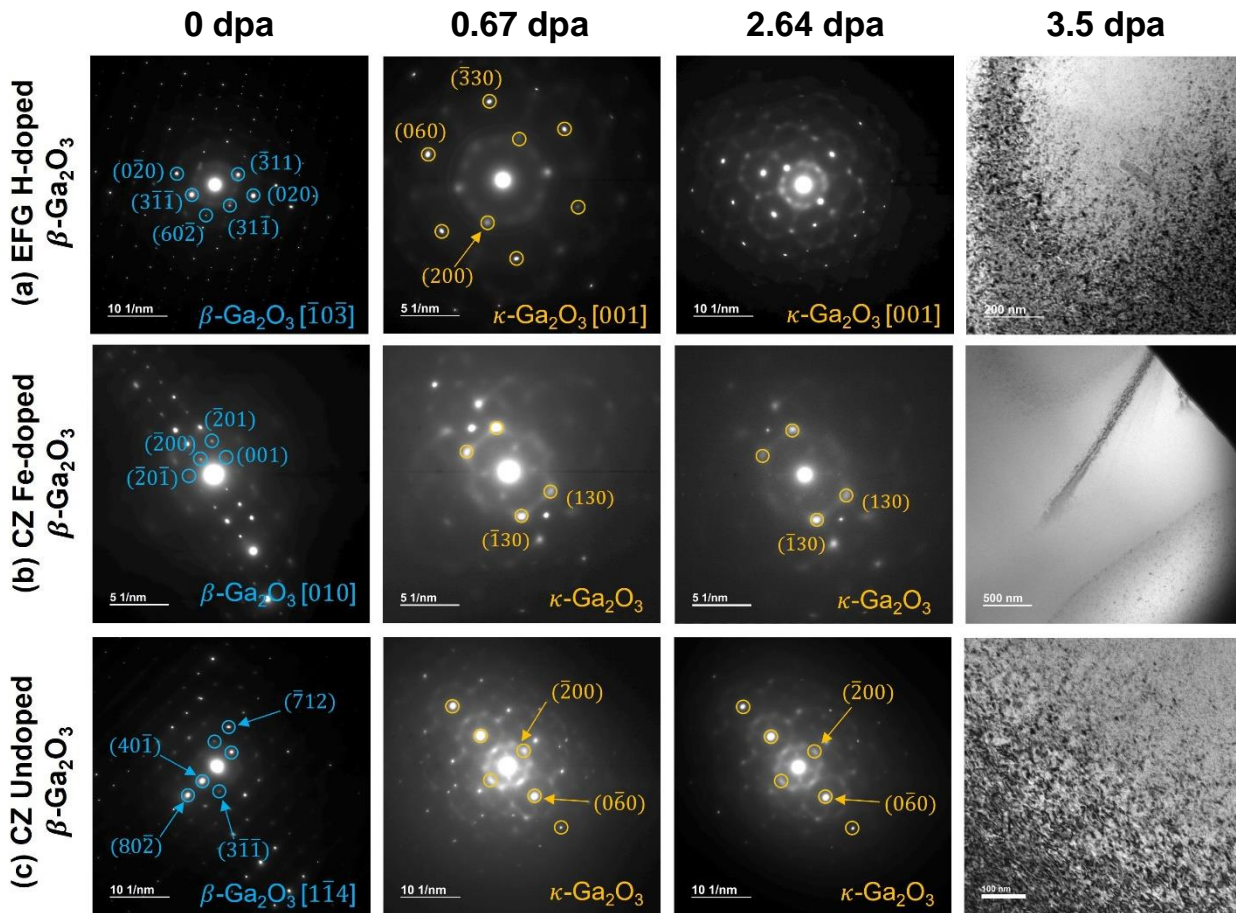


Figure 4.1 Sequence of electron diffraction patterns and bright field image acquired for (a) CZ β -Ga₂O₃ Fe-doped, (b) EFG β -Ga₂O₃ H-doped, and (c) CZ β -Ga₂O₃. Experiments and TEM done by Dr. Angelica Lopez [22]

Here, the irradiation damage on the samples can be described by the formation of black dots on the Bright Field images and the formation of resolvable dislocation loops as presented in Figure 4.1 with a rather lower density of loop formation in the Ga₂O₃ Fe-doped sample. Upon irradiation, the diffraction patterns of the crystals started to change. At dose as low as 0.67 dpa, the SAED patterns that were acquired in-situ showed a distinctive configuration that resembles a flower pattern with hexagonal symmetry. These changes in the SAED of the samples advocate that a phase transformation has begun to take place. The SAED that were acquired from 0.67dpa-3.5dpa for each of the three gallium oxide samples and shown in figure 4.1 were initially indexed as κ -Ga₂O₃. However, many of the spots were left unindexed because it was not clear at the time what phase they corresponded to. To obtain clearer diffraction patterns to supplement the initial patterns, a post irradiation examination of the samples was performed. The samples were tilted to find a common zone axis that could be used to identify the phases more easily as shown in figure 4.2. As identified by the full indexation of the EFG H-doped sample in figure 4.3, it appears that the two samples presented a mixed phase comprised of the γ -phase and κ -phase.

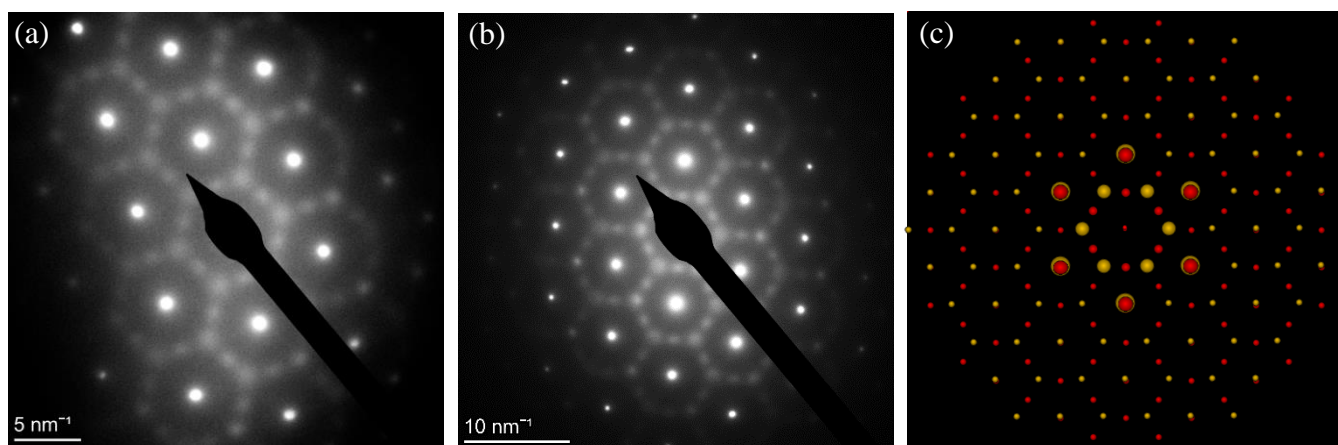


Figure 4.2 Selected area electron diffraction patterns from post irradiation examination of (a) CZ Fe-Doped Ga₂O₃, (b) EFG H-Doped Ga₂O₃, and (c) a simulation overlaying the [001] κ -Ga₂O₃ (orange) and [111] γ -Ga₂O₃ (red)

The two patterns overlaid on one another account for all the spots on the experimental patterns. Also, at the center of each hexagon lies a shared spot between the two phases with d-spacing values so close to one another that they overlap resulting in the summation of their intensities.

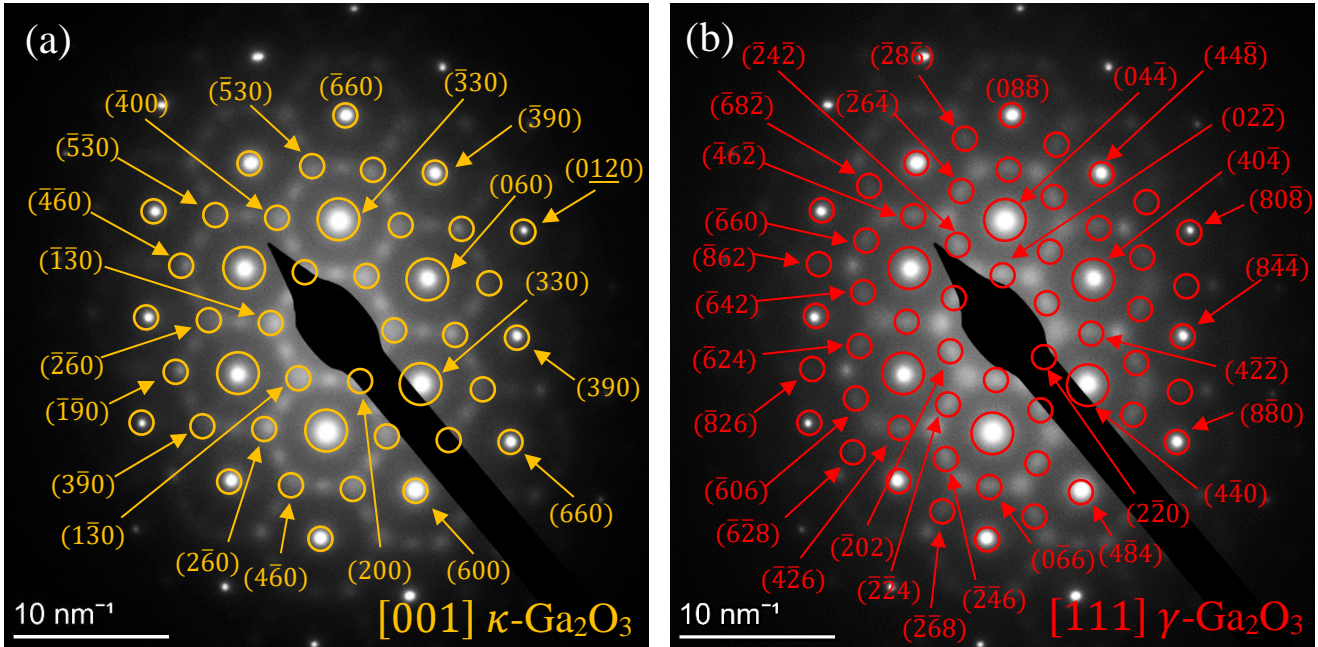


Figure 4.3 Full indexation of the κ -phase (a) and γ -phase (b) for the EFG H-doped sample irradiated to 3.5dpa at room temperature

A diffraction pattern for the CZ undoped sample is not shown in figure 4.2 with the other two samples. This is because that same zone couldn't be found during the post irradiation examination due to limitations of the β -tilt in the TEM. However, diffraction patterns were taken on different zones in this CZ undoped sample during post irradiation characterization. One of these zones is shown in figure 4.4a along with a simulation of the dual phase pattern in figure 4.4b. The bright spots still represent shared spots between the two phases and the diffused spots in between are unique to the γ -phase. Considering both the diffraction patterns for the CZ undoped sample in figure 4.1 as well as the on-zone pattern from the post irradiation examination in figure 4.4, a phase transformation to a mixture of κ and γ is validated. This verifies that all three samples underwent the same phase change at around the same dose.

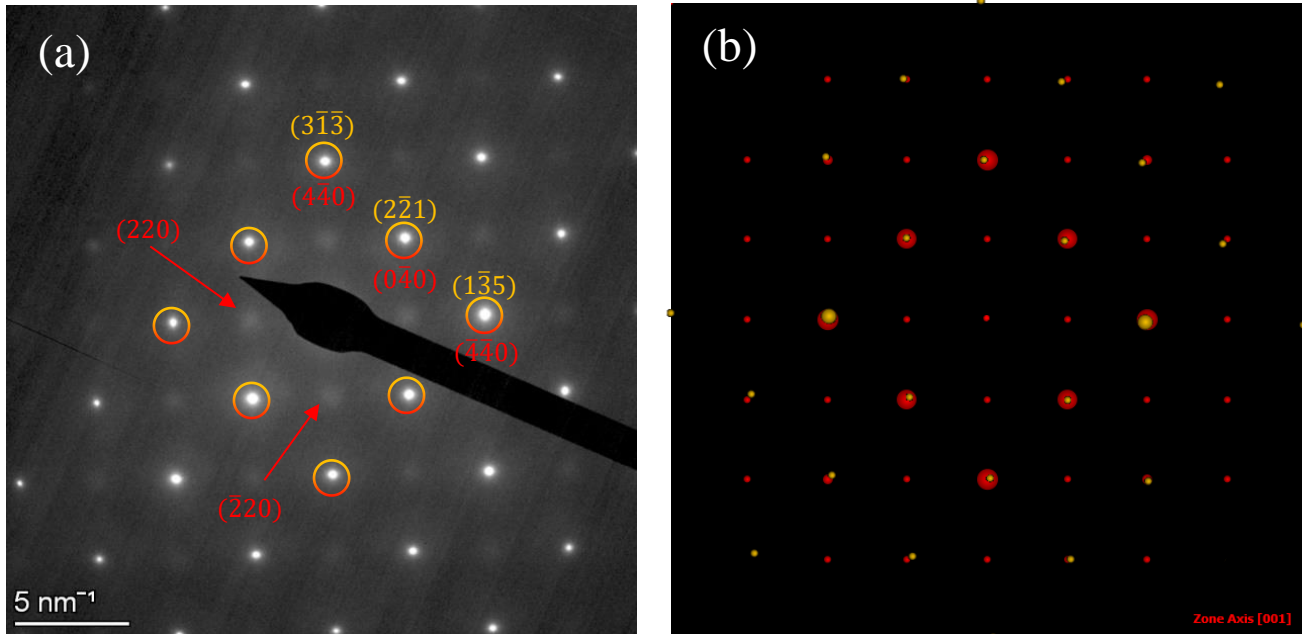


Figure 4.4 (a) Full indexation of the κ -phase (orange) and γ -phase (red) for the CZ undoped sample irradiated to 3.5dpa at room temperature and (b) simulation of [001] γ -phase and [794] κ -phase patterns overlaid on one another

Electron energy loss spectroscopy (EELS) was also done by Dr. Lopez to help identify if changes occurred by comparing spectra before and after irradiation. The O-K spectra from the CZ undoped and EFG H-doped samples before and after irradiation are illustrated in Figure 4.5. Here, it could be appreciated that O-K presents two major peaks that had been designated as O_1 and O_2 in Figure 4.5 a and b. These two fundamental peaks had been related to O 2p–Ga 4s and O 2p–Ga 4p band transitions, respectively [3]. Notice that in the non-irradiated samples the intensity ratio of those two peaks O_1 and O_2 is much larger compared to the intensity ratio of the irradiated samples. As explained in reference [3] these decreases in the difference in intensity between O_1 and O_2 is related to the formation of the new phase and can be attributed to either the increase in O 2p–Ga 4p hybridization or to the transfer of electrons from O 2p–Ga 4p band into another band.

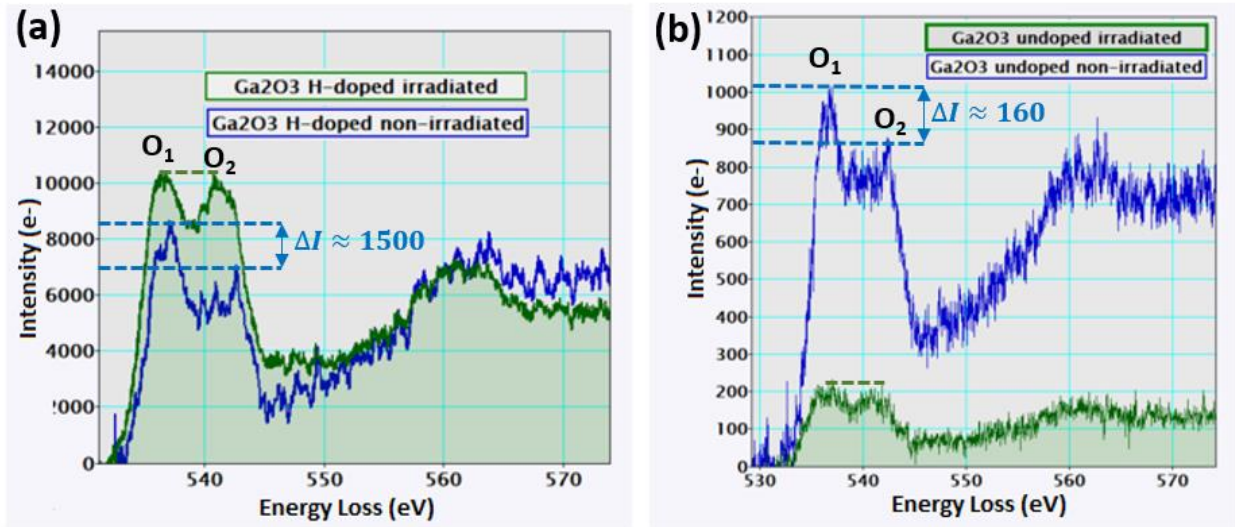


Figure 4.5 EELS spectra of the oxygen K edge, acquired from (a) unirradiated β -Ga₂O₃ H-doped and corresponding irradiated sample (b) unirradiated β -Ga₂O₃ undoped and corresponding irradiated sample. EELS done by Dr. Angelica Lopez [22]

The β -to- γ/κ transformation took place at a very low dose and the SAED that were acquired at successive doses did not present any other major changes which indicates the γ/κ phase seems to be very stable under further damage. This implies that while the disorder induced during the irradiation with the Kr ions up to a dose of 3.5dpa is enough to ignite β -to- γ/κ , it falls short of initiating the β -to- α or κ -to- α phase transitions. In addition, diffraction patterns were taken from the gallium oxides samples two years after the experiments were performed revealing that no recovery takes place over time (Figure 4.6). This indicates that the γ/κ -metastable phase, once formed, is indeed very stable not only with further irradiation but also through time.

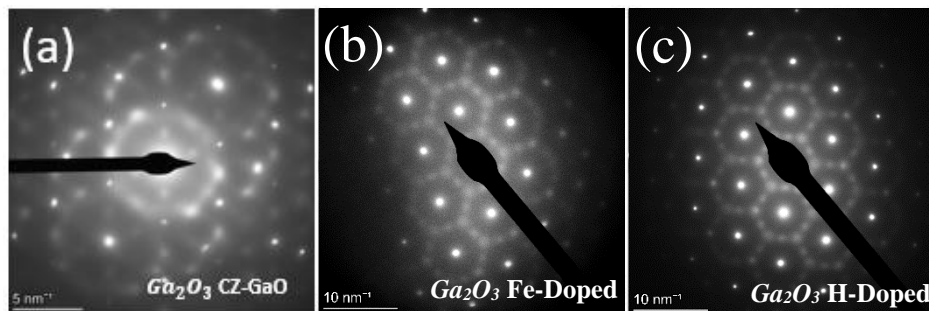


Figure 4.6 SAED acquired for the gallium oxide samples irradiated with 1 MeV Kr ions at RT (a) SAED corresponding to the initially β -Ga₂O₃ CZ-Ga₂O₃ sample (b) SAED corresponding to the initially β -Ga₂O₃ Fe-doped and (c) SAED corresponding to the initially β -Ga₂O₃ H-doped acquired one year after the experiment was performed.

Although the pattern in figure 4.6a does not have the same symmetry as the other two, a similar pattern is indexed later in the analysis in figure 5.2 as a mixture of the κ - and γ -phases as well.

4.2 High Temperature Results

4.2.1 CZ Undoped

The undoped CZ sample was first imaged at room temperature, and electron diffraction patterns were taken that determine the initial phase of the sample to be β -Ga₂O₃. Figure 4.7 shows that the sample is a single crystal. After taking initial electron diffraction patterns, the sample was heated to 300°C and irradiated to 4.03dpa. Diffraction patterns were taken throughout the irradiation to observe change. Figure 4.7 also shows diffraction patterns that were taken before and after irradiation. Using ImageJ supplemented with the Crystal Maker application, Single Crystal, the patterns were both indexed as β -Ga₂O₃ in the [101] direction. This means that no phase change occurred throughout the irradiation of the sample.

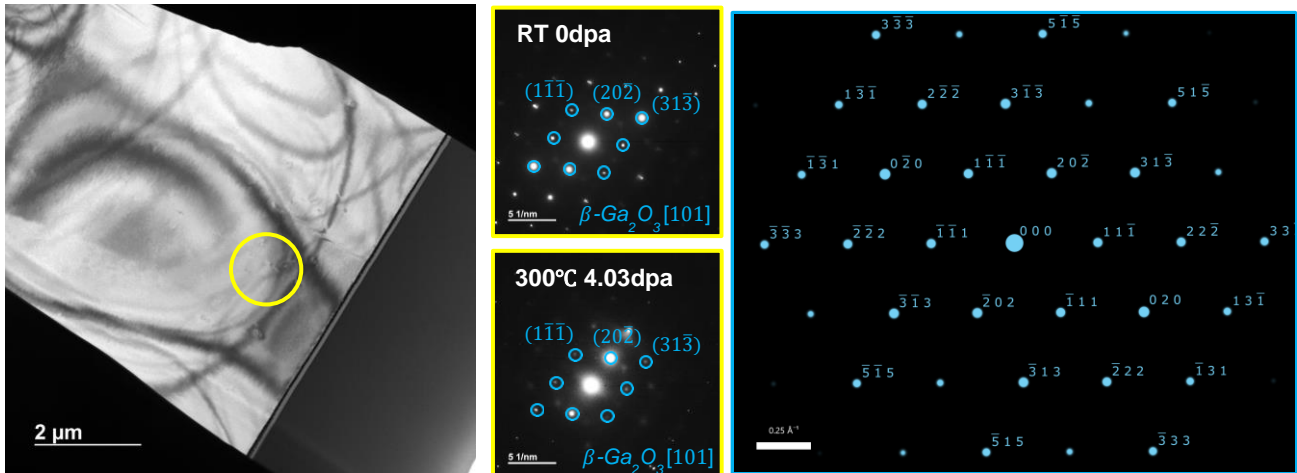


Figure 4.7 Diffraction patterns for CZ grown undoped Ga₂O₃ along with Single Crystal β -Ga₂O₃ pattern with zone axis [101]

4.2.2 CZ Fe-Doped

The CZ Fe-Doped sample was irradiated at an intermediate temperature of 150°C because the phase change behaviors above and below this temperature differed. In figure 4.8, brightfield TEM

images and diffraction patterns of the sample at room temperature reveal that it is also single crystal, single phase β -Ga₂O₃. Subsequently, the sample was heated to 150°C and irradiated to 4.0 dpa. Diffraction patterns at 4.0 dpa indicate that the material has undergone the same phase change as the room temperature samples. The red spots correspond to the [111] zone axis pattern for γ -Ga₂O₃, while the orange spots align with the [001] pattern for κ -Ga₂O₃. The spots that are circled in a gradient of red and orange are shared spots that appear in both patterns. The d-spacing for these spots are so close to one another (~1%) that they overlap on the diffraction pattern. It can be determined that the irradiation at 150°C created a mixed phase in the single crystal sample of γ -Ga₂O₃ and κ -Ga₂O₃ as the temperature was not high enough to suppress the change.

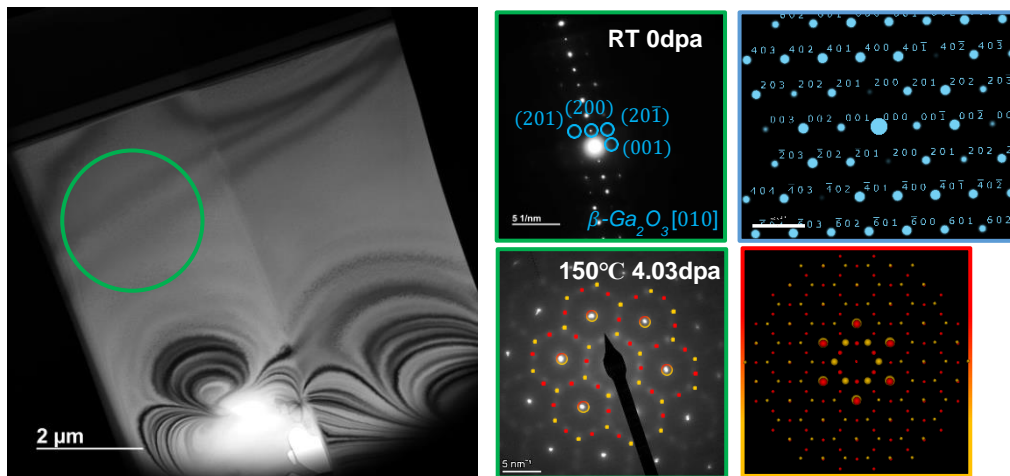


Figure 4.8 TEM image with indicated selected area (left), electron diffraction patterns (middle), and Single Crystal© patterns of corresponding β -Ga₂O₃ and κ -Ga₂O₃ (right) for CZ Fe-Doped sample

4.2.3 EFG H-Doped

Two different experiments were conducted on EFG H-Doped Ga₂O₃. In the previous experiments it was determined that the phase change at room temperature occurs around 0.55 dpa. To see the temperature effects, the first experiment was done at 300°C. Diffraction patterns were taken at room temperature and 300°C to confirm the phase of the gallium oxide. The material was then irradiated up to 6.74 dpa. Figure 4.9 shows the evolution of the diffraction patterns with increasing dose. The phase appears to remain as β -Ga₂O₃ in the [15 $\bar{8}$] direction throughout the irradiation

Chapter 5: Discussion

5.1 Verification of Phase Change

The changes that occur in the diffraction patterns throughout irradiation present compelling evidence of a phase transition. Another piece of evidence that the β -phase transforms to a new phase lies in the evolving bond structure observed under irradiation. This information came from the EELS spectra acquisition for both pristine gallium oxide samples and their irradiated counterparts, including the undoped CZ grown and H-doped samples. Band transitions are associated with peaks by correlating the amount of energy an electron loses to a specific band transition. The peaks, O_1 and O_2 , represent the $O2p - Ga4s$ and $O2p - Ga4p$ band transitions respectively as previously stated. The decrease in the difference in intensity of these peaks can either be interpreted as an increase in electrons undergoing the $O2p - Ga4p$ band transition or a decrease in electrons undergoing the $O2p - Ga4s$ band transition. This reveals that there is a change in electronic configuration which is most likely occurring from a change in crystal structure/phase. With the changing diffraction patterns in tandem with the EELS results a phase change of some sort is validated. The undetermined result at this point becomes the identification of this phase change.

Previous studies have had differing TEM DP indexation of the phase change of Ga_2O_3 under ion irradiation. Most studies reproduce the same hexagonal pattern that is characteristic of this material after ion irradiation in the zone axis $[001]$ for $\kappa/$ $[111]$ for γ ; the difference between the studies comes from the analysis of this pattern. In the first study done by Azarov et al., which implanted single crystals of β - Ga_2O_3 with 400 keV Ni ions at room temperature over a wide dose range of $6 \times 10^{13} - 1 \times 10^{16} \text{ cm}^{-2}$ (~ 0.14 - 21.95 dpa) [3], it was concluded that the hexagonal pattern resulting

from irradiation was purely κ -Ga₂O₃. Their analysis pointed out the correct zone axis for the κ -Ga₂O₃ pattern as [001], however the spots were improperly indexed.

Another study done by Garcia-Fernandez et al. implanted bulk Ga₂O₃ with Ni and Si ions [23]. This bulk irradiation resulted in a boundary between the damaged and undamaged layers at the depth of penetration of each ion in the same way as the study by Azarov. Diffraction patterns taken in the transformed layer showed multiple zone axes indicating that β transformed into the γ -phase. This differs from the indexation in our study as it is said to be pure γ -Ga₂O₃ rather than a mixture. The main experimental difference to notice is that these samples were irradiated as bulk samples meaning that the SAED can be taken perpendicular to the direction of ion incidence rather than along the incident ion direction, as is the case for in-situ irradiation. The pattern that was taken at the boundary between transformed and untransformed Ga₂O₃ was more similar to the diffraction obtained in our in-situ experiments. Indexation differed from the our study as it was interpreted as a mixture of [111] γ -Ga₂O₃ and three 120° rotated [111] β -Ga₂O₃ patterns [22]. The presence of β was explained by the pattern being taken at the boundary. The superposition of three β [111] patterns was explained by twinning that occurs on the boundary between implanted and un-implanted. Efforts were put into trying to re-index the pattern found in their publication [22] and upon simulation the three [111] β patterns rotated 120° from one another did not account for all spots on the pattern. In contrast, as previously shown in figures 4.2 and 4.3, the indexation in the current study as a mixture of [001] κ -Ga₂O₃ and [111] γ -Ga₂O₃ accounted for all spots on the experimental SAED.

To verify that this phase change is, in fact, a change to a mixture of κ and γ , another zone axis from a transformed sample was indexed. For this purpose, the CZ grown, Fe-doped sample that was irradiated at 150°C was re-examined. Figure 5.1 shows two diffraction patterns taken from

this sample. The hexagonal pattern has already been identified to be a mixture of the two phases, κ and γ . However, the pattern on the left which was taken from a different zone exhibits a new symmetry. This new pattern was indexed as a combination of the $[4\bar{1}\bar{7}]$ κ -phase and the $[011]$ γ -phase with the orange spots representing κ and the red spots representing γ shown in figure 5.2.

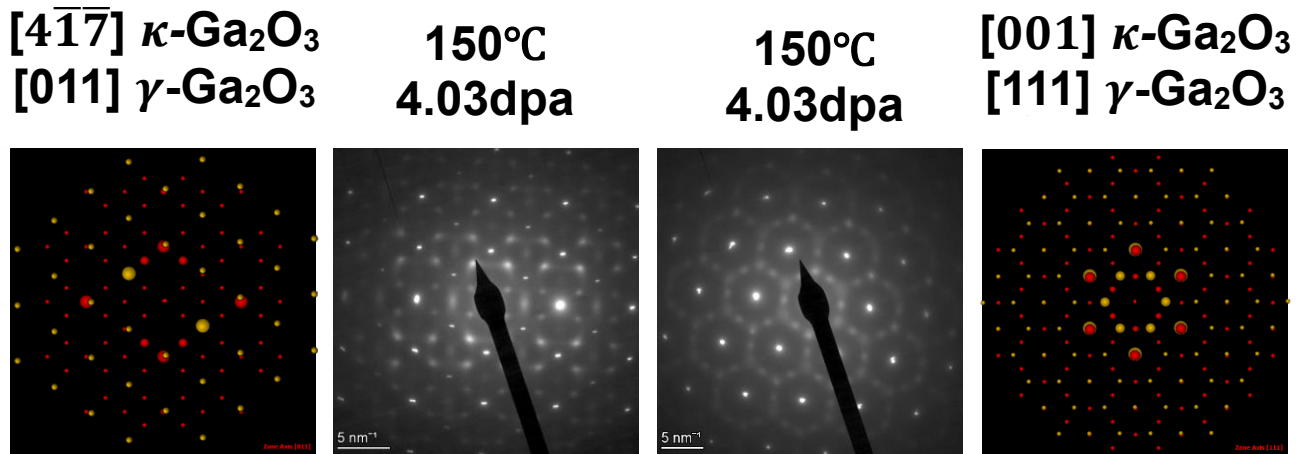


Figure 5.1 Experimental patterns on different zone axes from the CZ Fe-doped sample irradiated to 4.03dpa at 150°C along with simulated patterns of mixed κ -Ga₂O₃ (orange) and γ -Ga₂O₃ (red)

The simulated $[4\bar{1}\bar{7}]$ κ and $[011]$ γ indicate that there is a difference in d-spacing of the shared spots between the two phases. This was verified on the experimental pattern by looking at the shape of the bright spots. For example, looking closely at the $[280]_{\kappa}$ g-vector and $[800]_{\gamma}$ g-vector on the experimental pattern, two separate spots can be seen with a slight overlap. Another indication that there are two phases present is the intensity of the spots. If two spots on a pattern are overlapping their intensities are cumulative which makes the shared spots appear brighter than the rest.

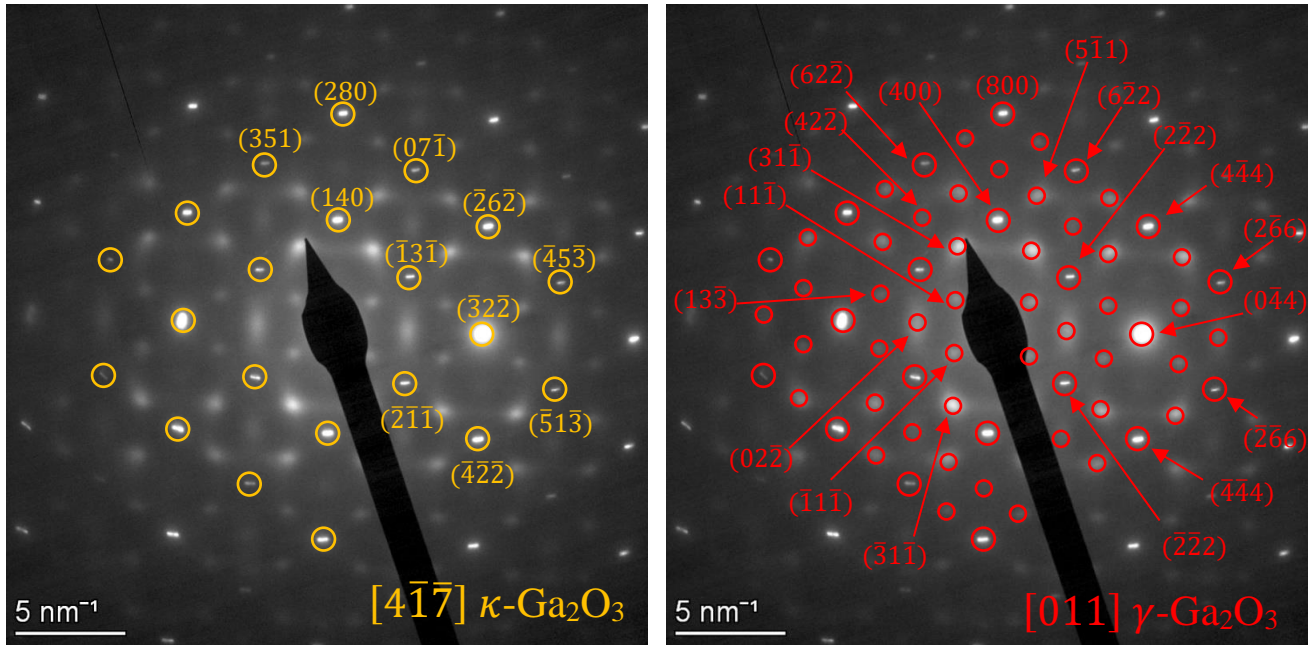


Figure 5.2 Full indexation of different zone axis pattern for CZ Fe-doped sample irradiated to 4.03dpa at 150°C

A final way to verify this phase change is by looking at the free energy of formation for the pristine and damaged states of the phases in question. A density functional theory (DFT) calculation done by Azarov et al. yielded a plot showing the total lattice energy vs. the volume per formula unit for all six phases of Ga_2O_3 [3] as shown in figure 5.3. In this case, a formula unit is one complete molecule of Ga_2O_3 . Using the volume of the unit cell and dividing by the number of molecules inside of the unit cell, a volume per formula unit value can be found that can be called specific volume. This value can be translated into a value of lattice energy per formula unit. As a material is bombarded with ions, the atoms in the lattice are knocked out of position changing the amount of formula units per unit cell volume. The unit cell volume remains constant so it can be inferred that an accumulation of vacancies in a unit cell would decrease the amount of formula units and therefore raise the specific volume. A monoclinic $\beta\text{-Ga}_2\text{O}_3$, unit cell has around 3.8 formula units with a volume of 209.6 \AA^3 giving it a specific volume of $55 \text{ \AA}^3/\text{f.u.}$ This makes sense as it is the undamaged state of $\beta\text{-Ga}_2\text{O}_3$ and it sits right at the minimum in figure 5.3. If we consider that one formula unit, or one molecule, of Ga_2O_3 is knocked out of a β -phase unit cell, with only 2.8

formula units left the new specific volume becomes $\sim 75 \text{ \AA}^3/\text{f.u.}$ Following the $\beta\text{-Ga}_2\text{O}_3$ curve on the plot this new specific volume leads right to the intersection with the γ -phase. This means that anything higher than one formula unit being displaced in a unit cell will lead to the γ -phase becoming the more energetically favorable state. However, when a sample is being irradiated the displaced atoms cannot simply disappear, the atoms may be relocated in other regions of the sample as interstitials or filling vacant site. Figure 5.4 shows a very simplistic theoretical scenario involving a system containing only two unit cells of $\beta\text{-Ga}_2\text{O}_3$, subject to irradiation from a single direction. Before irradiation both cells are undamaged making the β -phase the most energetically favorable phase. At the end of irradiation, in this scenario, three oxygen atoms and two gallium atoms have been knocked from one unit cell to the other. This leaves the unit cell on the left with a lower amount of formula units than before and the unit cell on the right with a higher amount of formula units than before if a directional effect is considered following the ion incidence direction.

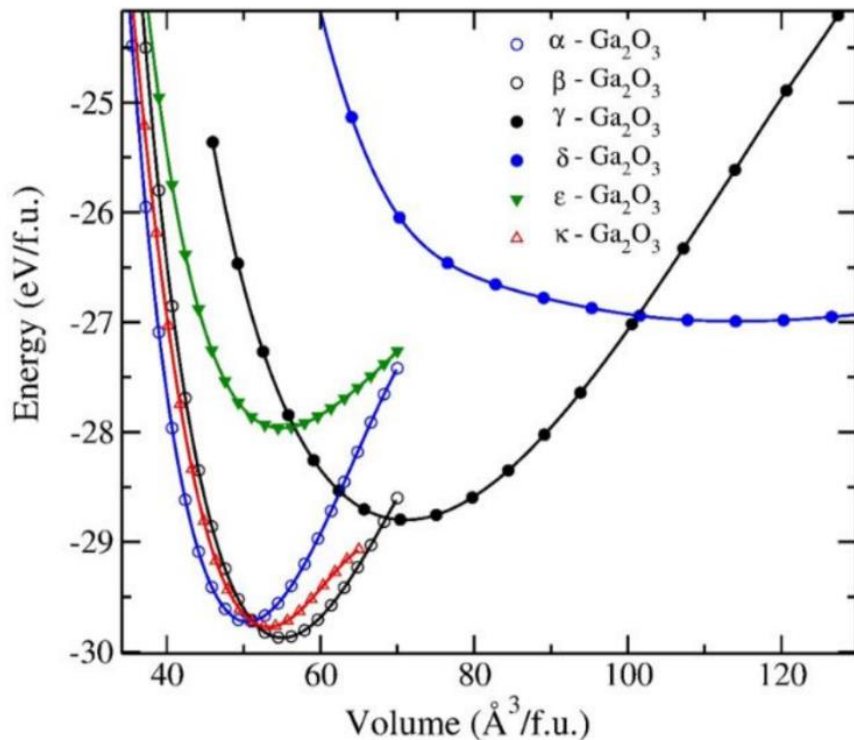


Figure 5.3 “Lattice total energy vs volume per formula unit for six different Ga_2O_3 polymorphs obtained with DFT calculations.” [3]

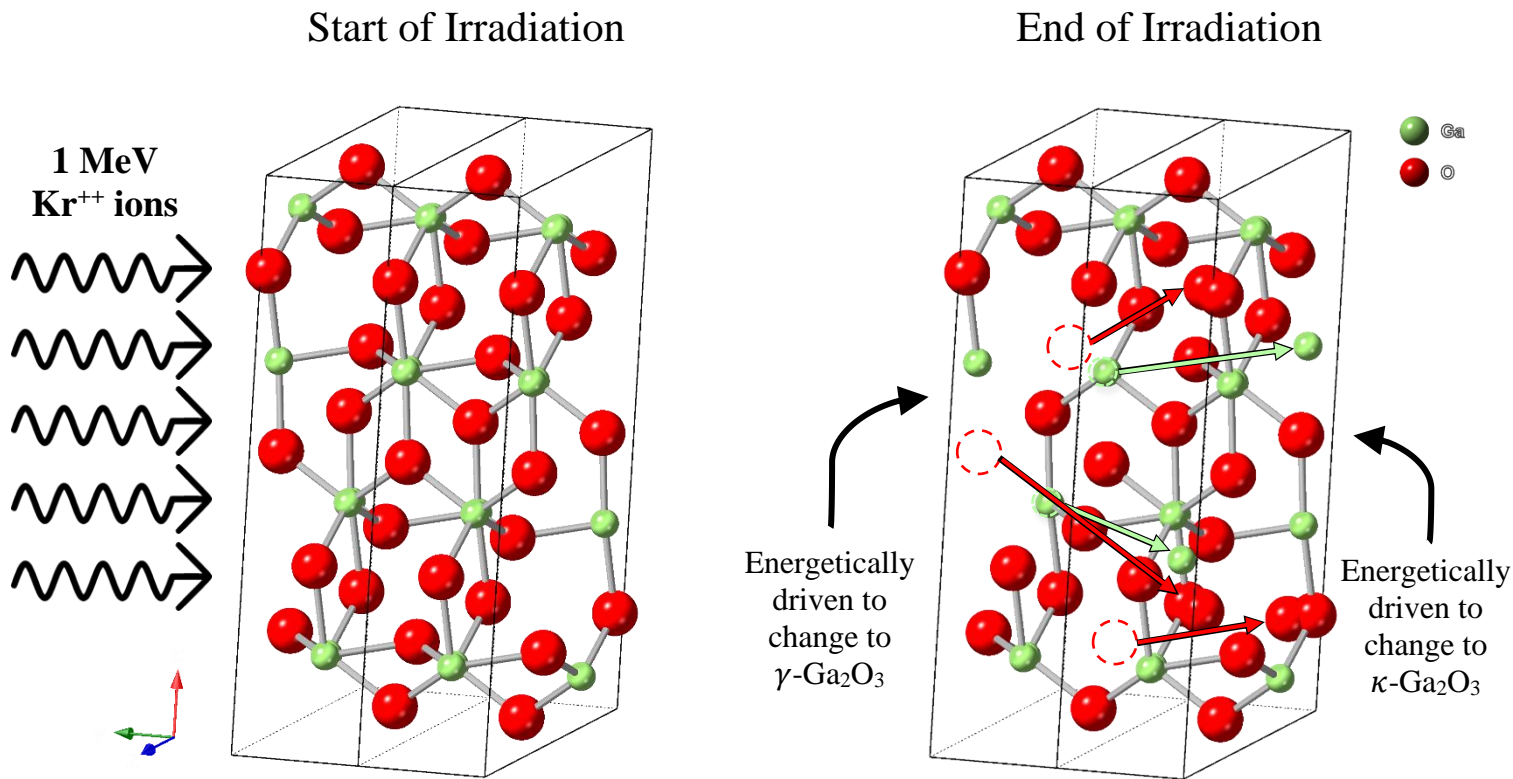


Figure 5.4 Theoretical scenario of two unit cells being irradiated with 1 MeV Kr ions. The two unit cells are shown in pristine condition at the start of irradiation (left) and in the damaged state after irradiation (right)

As previously discussed, the cell with a smaller amount of formula units would be energetically driven to transition to the γ -phase. Although, there is now an “overpacked” cell on the right which would decrease the specific volume of the cell. Following the β - Ga_2O_3 curve to the left meets an intersection between κ and β in which the κ -phase overtakes the β -phase as the most energetically favorable state. Theoretically this would leave the system with one κ unit cell and one γ unit cell, a mixed phase. It should be noted that the α -phase is lower energy than κ as you move to the left on the Gibbs free energy curves. The transition to κ - Ga_2O_3 instead of α - Ga_2O_3 can be explained by the metastable nature of the κ phase. This means that the microstructure can get “stuck” in the κ -phase and not be able to reach the lowest energy state. It may be more energetically stable, but the atoms may not be able to overcome the energy barriers to reach that phase. Also, the α -phase

was considered during indexation and was not found as a possible phase for the indexed patterns. It was found that in the [001] direction, the α and κ phases were almost indistinguishable from one another. However, looking at different zone axes, for example the patterns in figures 4.4 and 5.2, a matching zone for the α -phase could not be found.

Again, this scenario is an oversimplified version of a possible mechanism to explain the phase change to a mixed phase (especially when considering the number of cells considered). The irradiation induced phase change is affected by many different factors including charge neutrality. In a real crystal, you do not have exactly one formula unit of Ga_2O_3 being displaced from each unit cell. One way to maintain charge neutrality would be through the adaptation of charge state of the gallium ion. In addition, in a real crystal the damaged cells do not directly transform into different phases, rather they could act more like a precursor or nucleation site for the new phase. The γ -phase would build off of regions with a higher average of displaced atoms whereas the κ -phase would build off of regions with a higher average of accumulated atoms. The important concept is that the lattice will always be driven towards charge neutrality and minimum energy so in general, sub-stoichiometric regions would theoretically be driven to γ - Ga_2O_3 while hyper-stoichiometric regions would theoretically be driven to κ - Ga_2O_3 .

Other studies including one by Junlei Zhao et al. delved into the Gibbs free energy curves acquired through DFT. Zhao compared gaussian approximation potentials (GAPs), specifically tabulated low-dimensional GAPs (tabGAP) and smooth overlap of atomic positions GAPs (soapGAP), to their density functional theory simulations [24]. These GAP algorithms are both machine learning algorithms that are based on the framework of Gaussian process regression [24]. The results from the article that compare the Gibbs free energy curves for all six Ga_2O_3 polymorphs are shown in figure 5.5.

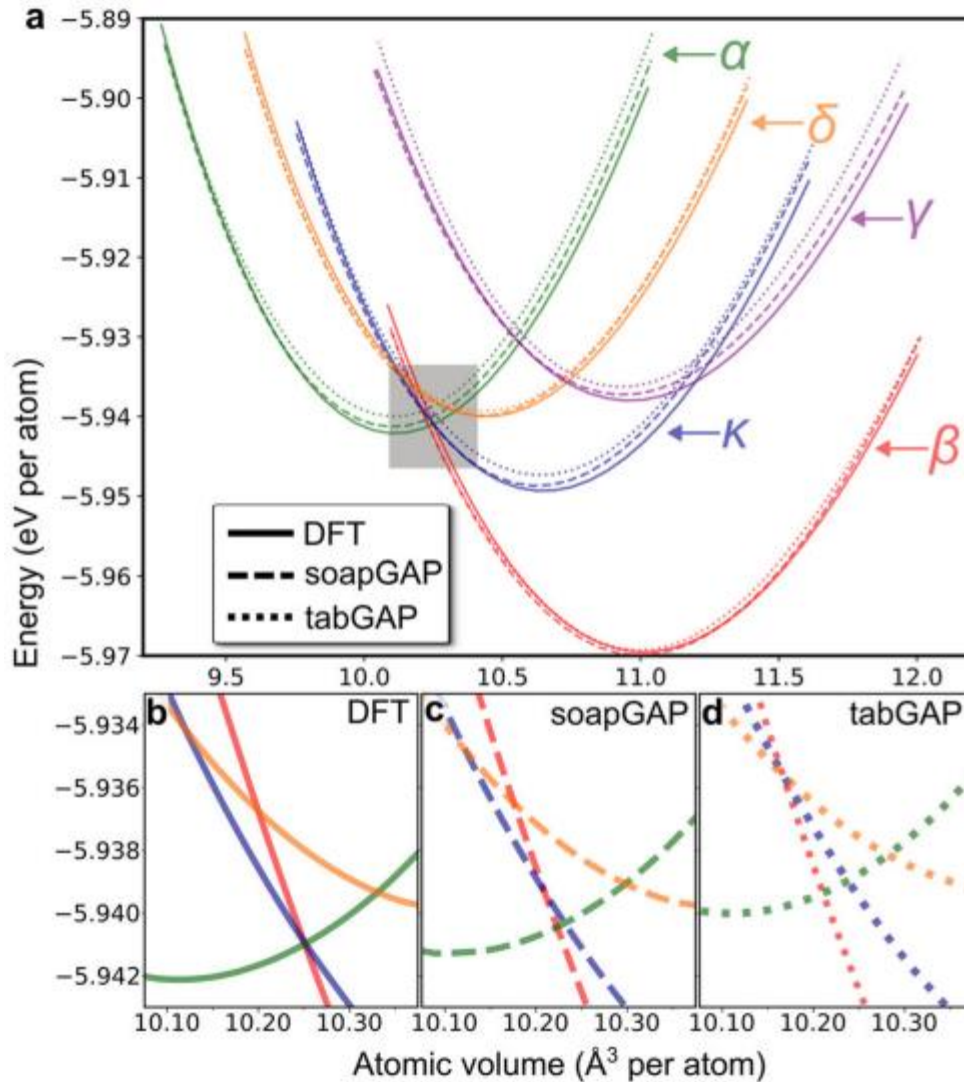


Figure 5.5 "Comparison of the DFT, soapGAP and tabGAP energies for the five experimentally identified $\beta/\kappa/\alpha/\delta/\gamma$ polymorphs. In the overall plot (a), the gray shadow region corresponds to the energy-crossing region magnified and compared closely in (b, c, d)." [24]

The GAP simulations had very little error compared to the density functional theory simulations.

The same crossover of the κ and β phases is present when following the β curve to the left as specific volume decreases. The same cannot be said for the γ and β crossover following the β curve to the right with increasing specific volume. Without knowing the parameters of the DFT calculations that were done in each of these studies one cannot comment on the accuracy of the shape of the curves. On the other hand, the specific volume of the minimum energy states for the phases can be determined using parameters of each crystal structure from their respective

crystallographic information files (CIF)[25]. Table 5.1 gives some crystallographic information for the phases in which data was available. All specific volume values are given for the undamaged crystal at its lowest possible energy state.

Table 5.1 Crystallographic information for Ga₂O₃ polymorph phases of interest

Phase	β	α	κ	γ
Structure	Monoclinic	Rhombohedral	Orthorhombic	Cubic
Space group	C2/m	R-3c	Pna21	Fd-3m
Atoms per unit cell	20	30	40	40 or 54
Unit Cell Volume [Å³]	209.55	288.80	407.45	556.2 or 555.4
Specific Volume [Å³/molecule]	52.39	48.13	50.93	69.53 or 51.43
Specific Volume [Å³/atom]	10.48	9.63	10.19	13.91 or 10.29

The γ -Ga₂O₃ crystallographic information is shown on the table as two possible values. A powder diffraction file (PDF) labeled 00-020-0426, entered into the database in 1970, reports the specific molecular volume of γ -Ga₂O₃ to be 51.43 [Å³/molecule], while a PDF labeled 01-083-7110, entered into the database in 2016 and modified in 2020, reports a specific molecular volume of 69.53 for γ -Ga₂O₃ [25]. Both PDFs report the structure to be cubic of space group Fd-3m with almost identical unit cell volumes. Using the experimental PDF data, the percent error of the specific volume for undamaged phases in both DFT simulations was calculated and displayed in table 5.2. Both curves are relatively accurate compared to the experimental data, but an interesting phenomenon arises with the γ curves. Experimental data suggests that the γ -phase can be present in two different states depending on the packing of the atoms. In one case the unit cell has 40 atoms

and in the other case the unit cell has 54 atoms which changes the specific volume of the phases. This suggests that the true γ free energy curve may be a mixture of the two curves shown in figures 5.3 and 5.5, or they may be two separate curves altogether. Both scenarios can support the previous hypothesis that if, by means of irradiation induced displacement of atoms there are regions of high and low atomic density (“overpacked” and “underpacked” cells), they can be energetically driven to form a κ/γ mixture due to the molecular volume of the γ -phase being $69.53[\text{\AA}^3/\text{molecule}]$ and the molecular volume of the κ -phase being $50.93[\text{\AA}^3/\text{molecule}]$.

Table 5.2 Error calculation for the specific volumes of undamaged Ga_2O_3 polymorphs found in figures 5.3 and 5.5 relative to experimental data in PDFs

Phase	%Error of Undamaged States in Figure 5.3	%Error of Undamaged States in Figure 5.5
β	5.12%	4.99%
α	4.82%	5.06%
κ	4.03%	4.54%
γ	2.18%*	6.61%*

5.2 Effect of Temperature

The effect of temperature becomes clear when comparing the results of the EFG grown H-doped samples. Three different tests were done at the following temperatures: 300°C, 100°C and room temperature. Figure 5.6 shows how the crystal structure is affected by irradiation at the various temperatures through changes in the diffraction pattern. The highest temperature, 300°C, shows no change in phase as the transition is completely suppressed.

* Based on the calculated specific volumes, the 1970 PDF data for the γ -phase was used to calculate % error for the DFT curve in figure 5.8, and the 2007 PDF data for the γ -phase was used to calculate % error for the DFT curve in figure 5.6

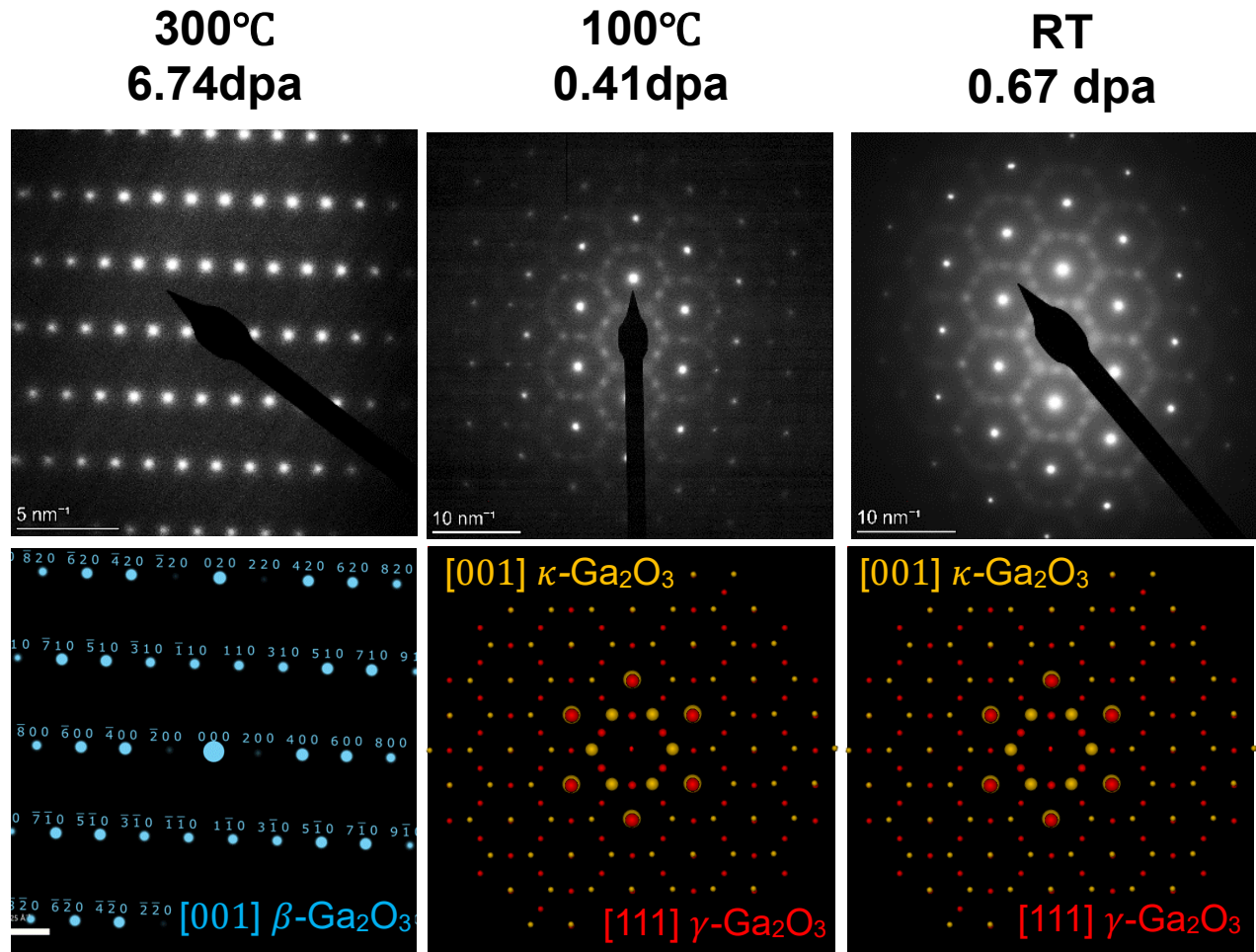


Figure 5.6 Comparison of diffraction patterns for EFG grown H-doped samples irradiated at 300°C, 100°C and room temperature along with simulated electron diffraction patterns for the indexed phases

The sample starts as $\beta\text{-Ga}_2\text{O}_3$ and the monoclinic structure remains stable throughout irradiation. The post irradiation pattern was indexed to be $\beta\text{-Ga}_2\text{O}_3$ in the [001] direction. The experiment done at room temperature underwent a complete transition to a mixture of $\gamma\text{-Ga}_2\text{O}_3$ and $\kappa\text{-Ga}_2\text{O}_3$. The experiment done at the intermediate temperature, 100°C, shows the same phenomenon as the room temperature experiment. The sample exhibited the same pattern of hexagonal symmetry that was identified as a mixed phase between γ -phase and κ -phase. This result suggests that 100°C is not a high enough temperature to suppress the phase change. This implies that the phase transformation is a result of two competing processes, the rate of production of defects (especially oxygen vacancies) due to irradiation competing with the rate of recombination between oxygen

interstitials and vacancies due to thermal annealing. If the temperature is not high enough, then the rate of vacancy creation is higher than the rate of thermal annealing which results in a transition in phase. In the case of the 300°C experiments, the rate of thermal annealing of vacancies was greater than the rate of creation so the phase change was completely suppressed. The critical temperature for the phase transformation is thus between 100°C and 300°C. More experiments are needed to fine tune this critical temperature.

5.3 Effect of Dopant

The initial interpretation of the room temperature results was that the EFG grown H-doped sample was the only sample that fully transformed during irradiation as it was the only sample to show full hexagonal symmetry. This brought about an idea that gallium vacancies were the mechanism by which the material changes phase. Hydrogen is positively charged, and gallium vacancies are negatively charged, so the idea was that the hydrogen atoms would sit in the gallium vacancies which would stabilize them by preventing any recombination [26]. This would raise the free energy of the system and allow it to transition more easily under irradiation as less energy would be needed to overcome the threshold energy of phase change. However, upon tilting to a specific zone axis, hexagonal symmetry was found in all samples. This means that the partially hexagonal patterns seen for the CZ undoped and CZ Fe-doped samples in figure 4.1 are just different zone axes of the transitioned mixed phase. This rules out the role of hydrogen as an influence on the phase change because all samples transitioned at around the same dose regardless of dopant. It also weakens the hypothesis that gallium vacancies are the mechanism for the phase change because theoretically the H-doped samples should have more stable gallium vacancies than the rest. Finally, it brought to light the importance of finding the correct zone axis when trying to identify the different phases of Ga₂O₃. Being off the zone axis explains why the diffraction patterns in the high temperature

experiments seem to have extra unidentified spots. Tilting the 300°C samples to zone axis after irradiation revealed clean β -Ga₂O₃ patterns and tilting the 100-150°C samples to the desired zone axis after irradiation revealed the clean hexagonal κ and γ mixed phase patterns.

5.4 Effect of Thickness

During fabrication, some of the samples were thinned in a certain way to obtain two windows of thickness on one sample. Initial thinning was done on the FIB down to around 100nm at which another thinning was performed on half of the lift out to 50nm. This gave a lift out that was 100nm thick on one half and 50nm thick on the other. The goal was to have a region thin enough for EELS and a thicker region to follow the radiation damage during the experiment (to alleviate for possible excessive loss of defects to the free surfaces of the foil); this also allowed to determine the effect of thickness on the irradiation behavior. The idea is that an increase in the ratio of free surface to bulk material would affect the movement of defects which directly affects the phase change. Diffraction patterns taken in the thick and thin regions of the samples revealed that both regions had the same behavior under irradiation. At 300°C the phase change was suppressed in both the thick and thin window and from RT to 150°C both windows underwent the same phase change at the same dose. From this result it can be interpreted that the diffusion of defects to the free surface was not substantial enough to suppress the phase change at room temperature up to 150°C.

5.5 Mechanism of Phase Change

Seeing as the strain induced by the implantation of ions is not the mechanism behind the phase change, the question remains as to what the mechanism is. In an attempt to recreate the phenomenon observed in the previously mentioned HfO₂ phase change study done by Mittman et al., a Ga₂O₃ film was grown by PVD RF magnetron sputtering on an NaCl substrate at LANL. The film was grown at 100W under an Ar flow of 30sccm with no oxygen being flowed into the

chamber with the expectation that this would result in a lower amount of oxygen than the stoichiometric equilibrium as some oxygen atoms are lost to the vacuum during oxide sputtering. The hypothesis was that the film would be present as γ -Ga₂O₃ instead of β -Ga₂O₃ due to the higher molecular volume resulting from oxygen loss. Unlike under irradiation, this sample should not be a mixed phase.

Indeed, while during irradiation, atoms that are displaced from one lattice site can move to other lattice sites or interstitial sites in the matrix resulting in regions of high- and low- molecular density, when growing a film with sub-stoichiometric amounts of oxygen, some oxygen atoms will be missing from their lattice positions, however these missing atoms are completely lost from the matrix instead of accumulating in other regions. This would result in a film with lower molecular density, or higher molecular volume, throughout. In our case, the as-deposited film was found to be amorphous using GI-XRD. Subsequently the film was heated to 800°C in-situ in a TEM and started crystallizing around 500°C. Figure 5.7 provides images and diffraction patterns of the film before and after crystallization. The initial diffraction pattern shows diffused amorphous rings with no sign of crystallinity. The diffraction pattern taken at 800°C, however, shows a nanocrystalline ring pattern that was indexed as γ -Ga₂O₃. To further investigate this indexation, SAED patterns were taken on single grains in different regions of the film. Bright Field TEM images and diffraction patterns are shown in figure 5.8 for these additional regions. The patterns are not as clean as the single crystal irradiated samples because the grains were too small to fit into a selected area aperture and tilt to zone axis. To alleviate this issue, the grains that were selected for diffraction were very dark in the TEM images meaning they were diffracting well and close to a zone axis. The patterns show multiple zone axes indexed as γ -Ga₂O₃. Neglecting spots from neighboring grains, the diffraction patterns indicate that the sample is crystallizing into single

phase γ -Ga₂O₃. This experiment supports the idea that oxygen vacancies are instrumental in the phase change mechanism. With a sub-stoichiometric amount of oxygen in the microstructure, the molecular volume increases and the lowest energy state becomes the γ -phase. Naturally, Ga₂O₃ wants to be in its most stable form, β -Ga₂O₃, but enough oxygen vacancies makes the β -phase too high in energy compared to γ .

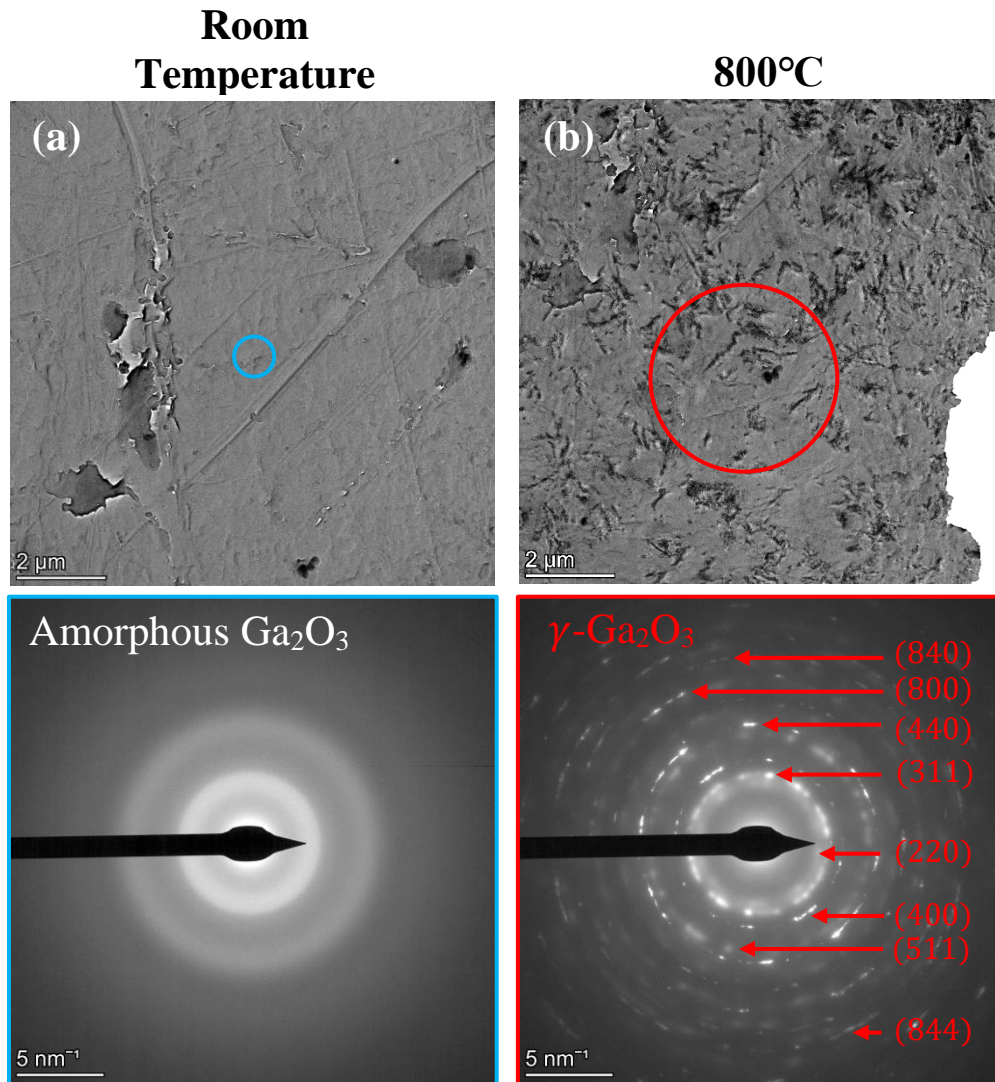


Figure 5.7 Low magnification bright field TEM images of Ga₂O₃ film at room temperature (a) and at 800°C (b) along with corresponding electron diffraction patterns

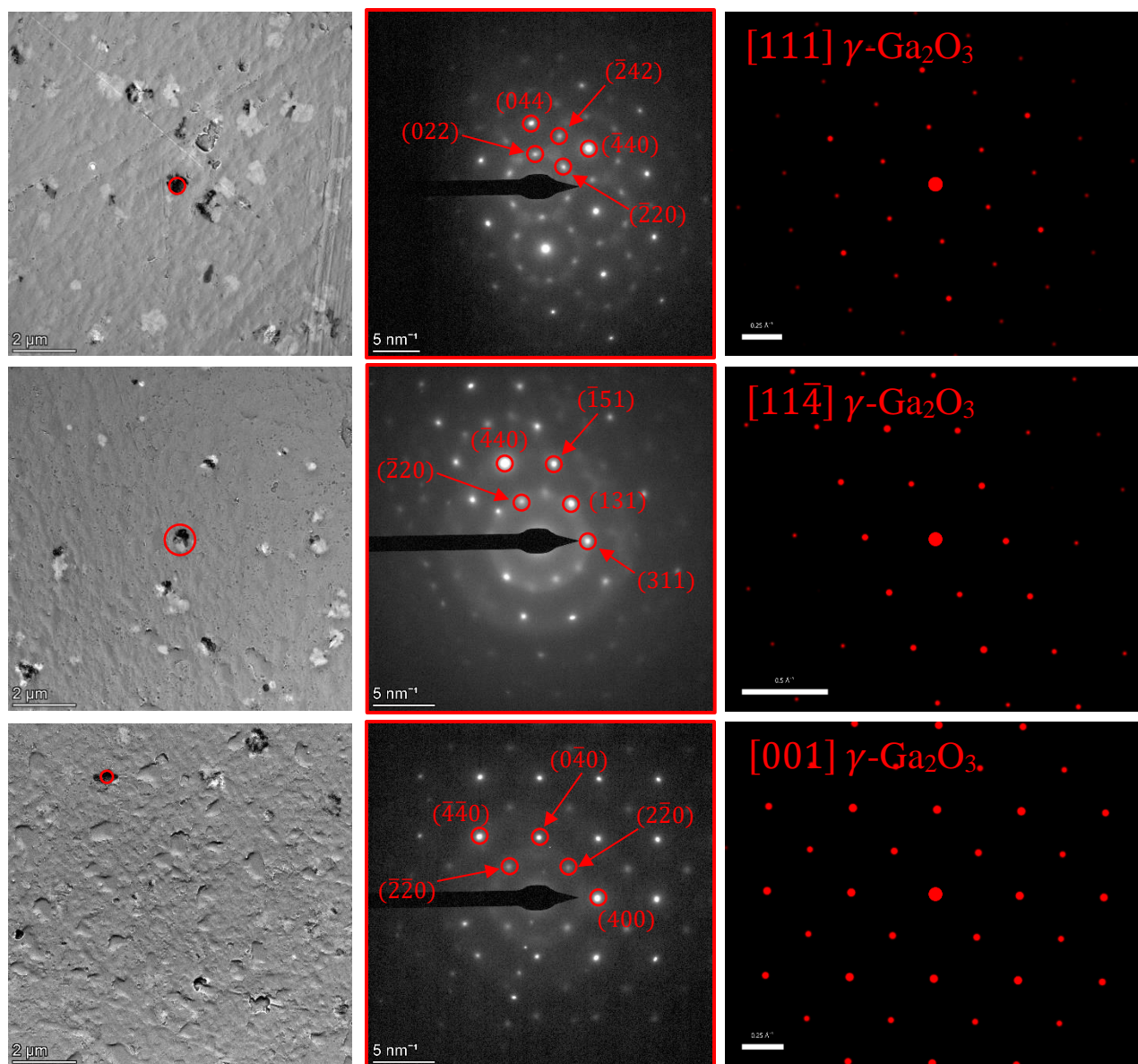


Figure 5.8 Low magnification bright field TEM images of different regions of Ga_2O_3 film at 800°C along with diffraction patterns and simulated diffraction patterns

This relates to the irradiation experiments because irradiation also accumulates high concentrations of oxygen vacancies. The difference is that the oxygen vacancies in the irradiated samples were created from high energy Kr^{++} ions displacing oxygen whereas the thin film was grown with less oxygen intentionally. During irradiation, the displacement of oxygen atoms is expected to happen on a more frequent basis compared to gallium atoms when considering the lower displacement threshold energy of 14eV compared to the displacement threshold energy of 28eV considered for

gallium, and also considering the higher atomic density of oxygen atoms compared to gallium atoms [21].

CHAPTER 6: Conclusion

One major conclusion of this study is the fact that β -Ga₂O₃ will readily undergo a phase change to a mixed phase composed of γ -Ga₂O₃ and κ -Ga₂O₃ under ion irradiation at room temperature. Tests done at 100°C and 150°C indicate that the same $\beta \rightarrow \gamma/\kappa$ phase change takes place around the same dose as the room temperature runs. From these experiments it can be concluded that the material will transition to the mixed phase as early as 0.65dpa from room temperature all the way up to 150°C. At 300°C, however, the phase change is fully suppressed. This suppression of the phase change at 300°C is most likely a result of two competing processes that occur in the material during irradiation at high temperature: creation of defects by means of ion irradiation and the thermal annealing of defects. At 150°C the rate of thermal annealing is not high enough to counteract the rate of defect creation resulting in a phase change. At 300°C the rate of thermal annealing is higher than the rate of defect creation, so the material shows no signs of phase change; it could be that defects are also lost in more significant ways to the free surfaces at 300C. The present study also points to the idea that oxygen vacancies are the species that play a major role in the the phase transformation mechanism.

Also, an important result of this study is the fact that the phase transformation is evidenced under in situ ion irradiation of a foil where the ions go through the foil and do not get implanted. This invalidate the hypothesis that the stress/strain induced by implantation of ions is needed for the transformation to happen as suggested in previous literature on the subject. If stress/strain is to play any role in the mechanism, then the stress/strain due to the irradiation damage alone would suffice since in this study ions are not implanted. A mechanism by which atomically overpacked and underpacked regions due to irradiation was suggested as a possible way to explain the formation of a mixed phase.

The results presented here also reveal a desirable amorphization resistance of Ga_2O_3 since no amorphization was observed for the irradiated samples to the doses reached in this study. The β -to- γ/κ transformation might play an important role in the amorphization behavior of gallium oxides by competing with / suppressing the amorphization with the polymorphic transformation. This likely opens a new field of the design and selection of compounds that are resistant to radiation damage and particularly to amorphization.

REFERENCES

1. Sharma, A., et al., *Nano-structured phases of gallium oxide ($GaOOH$, α - Ga_2O_3 , β - Ga_2O_3 , γ - Ga_2O_3 , δ - Ga_2O_3 , and ϵ - Ga_2O_3): fabrication, structural, and electronic structure investigations*. International Nano Letters, 2020. **10**(1): p. 71-79.
2. Cora, I., et al., *The real structure of ϵ - Ga_2O_3 and its relation to κ -phase*. CrystEngComm, 2017. **19**(11): p. 1509-1516.
3. Azarov, A., et al., *Disorder-Induced Ordering in Gallium Oxide Polymorphs*. Phys Rev Lett, 2022. **128**(1): p. 015704.
4. Yoshioka, S., et al., *Structures and energetics of Ga_2O_3 polymorphs*. Journal of Physics: Condensed Matter, 2007. **19**(34): p. 346211.
5. S.I. Stepanov, V.I.N., V.E. Bougrov, A.E. Romanov, *Gallium Oxide: Properties and Applications - A Review*. Reviews on Advanced Materials Science, 2016.
6. Pearton, S., et al., *Radiation damage in Ga_2O_3* . 2019: p. 313-328.
7. Shi, F. and H. Qiao, *Preparations, properties and applications of gallium oxide nanomaterials – A review*. Nano Select, 2021. **3**(2): p. 348-373.
8. Ai, W., et al., *Radiation damage in β - Ga_2O_3 induced by swift heavy ions*. Japanese Journal of Applied Physics, 2019. **58**(12): p. 120914.
9. Oshima, T., *Photodetectors*, in *Gallium Oxide: Materials Properties, Crystal Growth, and Devices*, M. Higashiwaki and S. Fujita, Editors. 2020, Springer International Publishing: Cham. p. 703-725.
10. Higashiwaki, M., et al., *Recent progress in Ga_2O_3 power devices*. Semiconductor Science and Technology, 2016. **31**(3): p. 034001.
11. Ueda, N., et al., *Synthesis and control of conductivity of ultraviolet transmitting β - Ga_2O_3 single crystals*. Applied Physics Letters, 1997. **70**(26): p. 3561-3563.
12. Cooke, J., B. Sensale-Rodriguez, and L. Ghadbeigi, *Methods for synthesizing β - Ga_2O_3 thin films beyond epitaxy*. Journal of Physics: Photonics, 2021. **3**(3): p. 032005.
13. *Springer Handbook of Electronic and Photonic Materials*, P.C. Safa Kasap, Editor. 2017, Springer International Publishing. p. 1536.
14. Srinivasan, K., *L10 Fe-Pt on Nanocrystalline HITPERM Soft Magnetic Underlayers for Perpendicular Recording Media*, in *Department of Materials Science and Engineering*. 2004, Carnegie Mellon University.
15. Cojocaru, L.N., *Defect-annealing in neutron-damaged β - Ga_2O_3* . Radiation Effects, 2006. **21**(3): p. 157-160.
16. Ahn, S., et al., *Effect of 5 MeV proton irradiation damage on performance of β - Ga_2O_3 photodetectors*. Journal of Vacuum Science & Technology B, Nanotechnology and Microelectronics: Materials, Processing, Measurement, and Phenomena, 2016. **34**(4).
17. Palade, C., et al., *A nanoscale continuous transition from the monoclinic to ferroelectric orthorhombic phase inside HfO_2 nanocrystals stabilized by HfO_2 capping and self-controlled Ge doping*. Journal of Materials Chemistry C, 2021. **9**(36): p. 12353-12366.
18. Mittmann, T., et al., *Stabilizing the ferroelectric phase in $HfO(2)$ -based films sputtered from ceramic targets under ambient oxygen*. Nanoscale, 2021. **13**(2): p. 912-921.
19. Argonne National Laboratory. IVEM: In situ Ion Irradiation; Available from: <https://www.anl.gov/ivem/ivem-in-situ-ion-irradiation>.

20. Stoller, R.E., et al., *On the use of SRIM for computing radiation damage exposure*. Nuclear Instruments and Methods in Physics Research Section B: Beam Interactions with Materials and Atoms, 2013. **310**: p. 75-80.
21. Tuttle, B.R., et al., *Atomic-displacement threshold energies and defect generation in irradiated β -Ga₂O₃: A first-principles investigation*. Journal of Applied Physics, 2023. **133**(1).
22. Morales, A.L., *Characterization of Ion Irradiation Effects in Fe₃O₄, α -Fe₂O₃, Cr₂O₃, α -Al₂O₃, and B-Ga₂O₃*, in *Nuclear Engineerign*. 2022, North Carolina State University
23. García-Fernández, J., et al., *Formation of γ -Ga₂O₃ by ion implantation: Polymorphic phase transformation of β -Ga₂O₃*. Applied Physics Letters, 2022. **121**(19).
24. Zhao, J., et al., *Complex Ga₂O₃ polymorphs explored by accurate and general-purpose machine-learning interatomic potentials*. npj Computational Materials, 2023. **9**(1).
25. Gates-Rector, S. and T. Blanton, *The Powder Diffraction File: a quality materials characterization database*. Powder Diffraction, 2019. **34**(4): p. 352-360.
26. Islam, M.M., et al., *Chemical manipulation of hydrogen induced high p-type and n-type conductivity in Ga₂O₃*. Sci Rep, 2020. **10**(1): p. 6134.